# INFORMATION TO USERS

This manuscript has been reproduced from the microfilm master. UMI films the text directly from the original or copy submitted. Thus, some thesis and dissertation copies are in typewriter face, while others may be from any type of computer printer.

**The quality of this reproduction is dependent upon the quality of the copy submitted.** Broken or indistinct print, colored or poor quality illustrations and photographs, print bleedthrough, substandard margins, and improper alignment can adversely affect reproduction.

In the unlikely event that the author did not send UMI a complete manuscript and there are missing pages, these will be noted. Also, if unauthorized copyright material had to be removed, a note will indicate the deletion.

Oversize materials (e.g., maps, drawings, charts) are reproduced by sectioning the original, beginning at the upper left-hand corner and continuing from left to right in equal sections with small overlaps.

Photographs included in the original manuscript have been reproduced xerographically in this copy. Higher quality 6" x 9" black and white photographic prints are available for any photographs or illustrations appearing in this copy for an additional charge. Contact UMI directly to order.

ProQuest Information and Learning
300 North Zeeb Road, Ann Arbor, MI 48106-1346 USA
800-521-0600

Université d'Ottawa · University of Ottawa

# EXPRESSION OF THE MURINE HOMOLOGUE OF XIAP (MIAP3) IN THE DEVELOPING MOUSE EMBRYO

Thesis submitted to the School of Graduate Studies and Research in partial fulfillment of the requirements for the degree of Master of Science

Department of Microbiology and Immunology, Faculty of Medicine
University of Ottawa, Ottawa, Ontario

By Suzana Drmanic

**Abstract**

Apoptosis or programmed cell death is a genetically controlled process that eliminates harmful or unwanted cells. This process plays an important role during development by contributing to tissue sculpting and in maintaining homeostasis of cell number in a variety of tissues. Recently, we have identified a family of apoptotic inhibitory proteins, *naip*, *hiap1* & *hiap2*, and *xiap*, which are capable of suppressing caspases, key proteolytic mediators of apoptosis. To elucidate a potential role for *xiap* during development, we have analyzed the expression patterns of the murine equivalent, *miap3*, at various stages of mouse development. *In situ* hybridization studies have revealed a ubiquitous expression pattern for *miap3* mRNA in a variety of developing organs, including brain, heart, lung, liver, pancreas, intestines and skin. Similar results were observed with wholemount *in situ* hybridization. In addition, immunohistochemical analysis demonstrated that *miap3* is widely expressed during embryonic days 9.5 to 16.5. Furthermore, *miap3* protein expression was observed in many of the adult mouse tissues and in day 9 to 13 mouse embryos by western blot analysis. These results demonstrate that *miap3* is ubiquitously distributed suggesting that it is an essential regulator of cell survival during murine development.

## ACKNOWLEDGEMENTS

I thank my supervisor Dr. Robert Korneluk for his tutelage and support during these studies. I also would like to thank Dr. Alex MacKenzie for his assistance. I thank my thesis committee members Drs. Ken Dimock, Dennis Bulman, and Lynn Megeney. I am also very grateful to Martin Holčik for providing the DNA templates, Keiko Hicks for the RIAP3 antibody she developed and for her technical advice, Connie Craig, and Peter Liston for their assistance. I would like to thank the CHEO and University of Ottawa Pathology Departments for their assistance, particularly Ute Davis and Mrs. Wong. Also, thanks to Dr. Luc Sabourin for the whole-mount *in situ* protocol and for his helpful suggestions. I am very appreciative for all the support that I have received from my lab mates, especially to Jennifer Ingram for the collaborative efforts made during both of our studies.

Special thanks to Chris Storbeck for his excellent technical advice and for the faith and encouragement he has provided me throughout these studies.

So many thanks to my mother, for her strong sense of belief in me and her never ending support and to my sister for her inspirational advice.

## TABLE OF CONTENTS

## LIST OF TABLES

**CHAPTER III: Results**

## LIST OF FIGURES

## LIST OF ABBREVIATIONS

| | |
|---|---|
| AP | alkaline phosphatase |
| APAF-1 | apoptosis protease activating factor-1 |
| ATP | adenosine triphosphate |
| Bak | Bcl-2 homologous antagonist/killer |
| Bax | Bcl-2 associated protein X |
| BCIP | 5-bromo-4-chloro-3-indolyl-phosphate |
| Bcl-2 | B-cell lymphoma 2 |
| BIR | Baculoviral Inhibitor of apoptosis Repeat |
| BMP | Bone Morphogenetic Protein |
| bp | base pair |
| BSA | bovine serum albumin |
| ° C | degree Celsius |
| CARD | Caspase Recruitment Domain |
| cDNA | complementary deoxyribonucleic acid |
| CNS | central nervous system |
| CSCl | cesium chloride |
| cpm | counts per minute |
| CTP | cytidine triphosphate |
| dATP | deoxyadenosine triphosphate |
| DCP-1 | *Drosophila* cell death protease-1 |
| DCP-2 | *Drosophila* cell death protease-2 |
| DD | death domain |

| | |
|---|---|
| $ddH_2O$ | double distilled water |
| DED | death effector domain |
| DIG | digoxigenin |
| DNA | deoxyribonucleic acid |
| dNTP | deoxynucleoside triphosphate |
| drICE | *Drosophila melanogaster* ICE protease |
| DRONC | Drosophila Nedd-2 like caspase |
| DTT | dithiothreitol |
| E | embryonic day |
| EDTA | ethylenediaminetetraacetic acid disodium salt |
| GTP | guanosine triphosphate |
| h | hour |
| $H_2O_2$ | hydrogen peroxide |
| HIAP1 | Human IAP1 |
| IAP | Inhibitor of Apoptosis Protein |
| ICE | interleukin-1β-converting enzyme |
| IgG | immunoglobulin G |
| IκB | Inhibitor kappa B |
| kb | kilobase |
| kDa | kilodalton |
| LB | Luria-Bertani medium |
| LiCl | lithium chloride |
| M | Molar |

| | |
|---|---|
| MeOH | methanol |
| min | minute |
| mg | milligram |
| $MgCl_2$ | magnesium chloride |
| ml | millilitre |
| mM | millimolar |
| mRNA | messenger ribonucleic acid |
| NaCl | sodium chloride |
| NAIP | Neuronal Apoptosis Inhibitor Protein |
| NaOH | sodium hydroxide |
| $NaPO_4$ | Sodium phosphate |
| ng | nanograms |
| NBT | nitroblue tetrazolium chloride |
| NFκB | Nuclear Factor kappa B |
| PAGE | polyacrylamide gel electrophoresis |
| PBS | phosphate buffered saline |
| PBT | 1X PBS with 0.1% Tween-20 |
| PCD | programmed cell death |
| PFA | paraformaldehyde |
| PMSF | phenylmethylsulfonyl fluoride |
| RNA | ribonucleic acid |
| rpm | revolutions per minute |
| RIAP3 | rat IAP3 |

| | |
|---|---|
| s | seconds |
| SDS | sodium dodecyl sulfate |
| SSC | standard saline citrate buffer |
| TAE | Tris acetate EDTA buffer |
| TGF- β | transforming growth factor- β |
| TNFα | tumour necrosis factor α |
| tRNA | transfer RNA |
| tris | tris (hydroxymethyl) aminomethane |
| U | units |
| μg | microgram |
| μl | microlitre |
| μm | micrometre |
| UTP | uridine triphosphate |
| UTR | untranslated region |
| UV | ultraviolet |
| XIAP | X-linked IAP |

# 1. Introduction

## 1.1 Apoptosis and development

The study of programmed cell death (PCD) or apoptosis has progressed partly due to the realization that normal development and homeostasis of metazoan animals requires precise regulation of cell death. As a result, cell death is now recognized as a vital component of animal development and tissue homeostasis. Normal cell death was initially observed during amphibian metamorphosis and was then identified in many of the developing organs in both invertebrates and vertebrates (Vaux and Korsmeyer, 1999). Consequently, there has been mounting evidence to suggest that cell death is a relatively conserved and essential process in the animal kingdom (Ellis et al., 1991; Vaux et al., 1992; Hengartner, 1994). Proof that a programmed mechanism did exist came from experiments showing that inhibitors of RNA and protein synthesis could suppress cell death, since re-expression of genes was required to initiate apoptosis (Tata, 1966; Lockshin, 1969; Oppenheim et al., 1990).

There are many different stimuli that are received extracellularily or intracellularily that may either restrain or favor PCD. The same signal, however, activating the apoptotic process in one cell type may have contradictory results in others. The term apoptosis originated from the observation that this form of cell death had particular morphological and biochemical characteristics (Kerr et al., 1972; Wyllie et al., 1980). More specifically, the apoptotic sequence of events include membrane blebbing, cytoplasmic shrinking, nuclear chromatin condensation, and nuclear fragmentation. Subsequently, cleavage of genomic DNA into small oligonucleosomal fragments is seen with the formation of membrane-bound bodies that are ultimately phagocytosed by

neighbouring cells or by macrophages without an inflammatory response (Kerr et al., 1972; Wyllie et al., 1980). It is well established that PCD executes many important functions during normal development, nearly all of which include the elimination of unwanted cells (Jacobson et al., 1997). It serves in the sculpting of developing structures, for example, as observed during the formation of the proamniotic cavity. The compact inner cell mass of the mouse blastocyst is converted into a hollow structure to produce lumina (Coucouvanis and Martin, 1995). Also, during later developmental stages, apoptosis aids in the removal of interdigital tissue (Zakeri and Ahuja, 1994). Furthermore, cell number is controlled in many of the embryonic tissues formed during development by eliminating the superfluous cells. For instance, extensive cell death is observed in the developing CNS of invertebrates and vertebrates, presumably involving neurons that fail to create the proper connections with their target cells. This results in the death of fifty percent of neural populations by apoptosis and thus eliminates superfluous cells (Oppenheim, 1991). In addition, PCD is also used to remove obsolete structures, misplaced, deleterious or nonfunctional cells and cells that are potentially dangerous to the animal. Although the mechanisms mediating cell death during mammalian development are poorly understood, genetic studies in simple organisms have provided model systems from which mammalian cell death mechanisms can be elucidated.

**1.2 Cell death during development of invertebrates**

During the study of development in the nematode, *Caenorhabditis elegans*, initial evidence for PCD was discovered. The identification of *ced-3*, a cell death effector, and *ced-4*, a regulatory protein functioning upstream of *ced-3*, were originally isolated through genetic studies performed in *C. elegans*. As a result, a first glimpse was provided

into the molecular mechanisms underlying the cell death program (Horvitz et al., 1982; Ellis and Horvitz, 1986). The *ced-3* gene encodes a cysteine protease homologous to the interleukin-1β-converting enzyme (ICE) family of proteases (caspases), that play a key role in executing the cell death cascade (Yuan et al., 1993). *Ced-4*, the activator of *ced-3*, has shown homology to the mammalian apoptosis protease activating factor-1 (Apaf-1) (Cecconi et al., 1998). In contrast, *ced-9* is an inhibitor of PCD in *C. elegans,* functioning upstream of *ced-3* and *ced-4* and is homologous to the mammalian anti-apoptotic protein Bcl-2 (Vaux et al., 1988; Hengartner and Horvitz, 1994; Korsmeyer, 1995). In the adult *C. elegans*, 131 of the 1090 somatic cells die by apoptosis. Therefore, loss of function mutations affecting either one of the initiators or effectors of PCD, *ced-4* or *ced-3*, would limit apoptosis (Yuan and Horvitz, 1992; Yuan et al., 1993). The contrary holds true for *ced-9*, where inadequate inhibition of cell death would permit the death of cells that would typically survive (Hengartner et al., 1992). The recent discovery of *egl-1*, a pro-apoptotic gene, appears to serve as the integration site of pro-apoptotic signals in *C. elegans* (Conradt and Horvitz, 1998). The *egl-1* protein resembles the Bcl-2 family of proteins, in view of its Bcl-2 homology domain (BH3 domain) and therefore may be part of the BH3 family of PCD activators. It has been recognized that Bcl-2 members with BH3 domains interact with one another. Accordingly, *egl-1* interacts with *ced-9* (Conradt and Horvitz, 1998). Therefore, the presumed model of cell death in *C. elegans* includes the binding of *egl-1* to *ced-9*, consequently inhibiting its activity, followed by the release of *ced-4* and *ced-3* from their inactive complex of *ced-9/ced-4/ced-3* (Bergmann et al., 1998; Conradt and Horvitz, 1998).

This fundamental mechanism of cell death observed in *C. elegans* is, to a varying

degree, similar in *Drosophila*. Cell death becomes more abundant at day 11 of embryogenesis, along with notably high levels detected in the central nervous system (CNS) at day 16 (Abrams et al., 1993). Apoptosis is also observed during *Drosophila* metamorphosis and is important in removing unnecessary structures. The three genes identified as *reaper* (*rpr*), *head involution defective* (*hid*), and *grim*, have been implicated in the regulation of apoptosis (White et al., 1994). Without exception, *reaper* and *grim* are expressed in cells that are destined to die, whereas *hid* appears to be expressed in cells that either die or survive (Meier and Evan, 1998). Moreover, the expression of these genes may be induced by various apoptotic stimuli and suggests that the integration of different apoptotic signals arises partially through a transcriptional mechanism (Bergmann et al., 1998).

The proteins of *reaper*, *hid*, and *grim*, have shown their ability to function upstream of caspases. In various cell types, most notably in the *Drosophila* compound eye, overexpression of these proteins have lead to the induction of apoptosis (Grether et al., 1995;White et al., 1996; Chen et al., 1996). However, co-expression of p35, a baculoviral inhibitor of apoptosis that specifically inhibits caspase proteases, prevents this cell death (Bump et al., 1995; Xue and Horvitz, 1995; Grether et al., 1995;White et al., 1996; Chen et al., 1996). This observation implies that *reaper*, *hid* and *grim* mediate cell death by activating the caspase pathway (Bergmann et al., 1998). Currently, four caspases have been identified in *Drosophila*, DCP-1, drICE, DCP-2/DREDD and DRONC. DCP-1 and drICE are comparable to *ced-3* and the mammalian family of effector caspases (Song et al., 1997; Fraser and Evan, 1997), while DREDD and DRONC are most similar to the mammalian initiator caspases (Inohara et al., 1997; Chen et al.,

1998; Dorstyn et al., 1999). Loss of function mutations in DCP-1 result in the death of most embryos during larval stages. In addition, female sterility is observed in the larvae that survive and therefore suggest that there may be some redundancy of *Drosophila* caspases or dependence on the maternally derived DCP-1 during early development (McCall and Steller 1998).

Despite the fact that homologs of *ced-9*/Bcl-2 have not yet been discovered in *Drosophila*, two inhibitor of apoptosis protein (IAP) genes have been identified, *diap1* and *diap2* (Hay et al., 1995). In addition, the mammalian counterparts have revealed their ability of binding directly to caspases and preventing their activation (Deveraux et al., 1997). Interestingly, the BIR (Baculoviral Inhibitor of apoptosis Repeat) motifs of baculoviral and *Drosophila* IAPs are capable of interacting with a 14 amino acid stretch present in the amino terminal region of *reaper*, *hid* and *grim*. This sequence is homologous in each of the respective proteins (Vucic et al., 1997 and 1998). Overexpression of *diap1* had suppressed cell death *in vitro* and loss of function mutations in *diap1* encouraged apoptosis induced by *reaper*, *hid* and *grim* (Hay et al., 1995). Moreover, *diap2* is repressed when steroid hormone ecdysone induces *reaper*, *hid* and *grim* to allow apoptosis in gut and salivary glands during metamorphosis of larval organs. However, as yet, it is not evident as to whether these IAPs suppress apoptosis by neutralizing these pro-apoptotic proteins or whether *reaper*, *hid* and *grim* provoke cell death by preventing the IAPs from impeding caspase activation. Since *reaper*, *hid* and *grim* interact physically with highly conserved IAP molecules, mammalian homologues of *reaper*, *hid* and *grim* must exist, although they have not yet been discovered. However, SMAC/DIABLO is a mitochondrial protein that assists cytochrome-c dependent caspase

activation by removing IAP inhibition and perhaps serves as a functional homologue (Du et al., 2000).

The cell death model systems of *C. elegans* and *Drosophila* have disclosed a fundamental cell death program that is exceptionally well conserved throughout evolution. The information accumulated from these systems has and will contribute to a further understanding of the complex mechanisms that exist during cell death in vertebrates.

## 1.3 Cell death in developing vertebrates

### 1.3.1 Caspases: critical components of the death machinery

Caspases are a family of cysteine proteases that are key mediators of the proteolytic cascade that is stimulated by various apoptotic triggers originating from outside or within the cell. They are known to cleave peptide substrates after aspartic acid residues (Alnemri et al., 1996). The cell death process is greatly suppressed by caspase inhibitors, implying that caspases are required for the execution of apoptosis (Nicholson and Thornberry, 1997). Presently, 14 mammalian caspases have been cloned and partially characterized (Kumar, 1999; Rathmel and Thompson, 1999). Caspases are located in the cell as inactive precursors (zymogens) and are activated upon proteolytic cleavage (between the domains). Once a death stimulus has been received, the zymogens are processed to produce a large subunit and small subunit that together create the active enzyme (Nicholson and Thornberry, 1997). The mammalian caspases that are involved in apoptosis are categorized into two groups. The first group consists of the initiator or upstream caspases, for example caspase-2, -8, -9 and –10, whereas the effector or downstream caspases include caspase-3, -6 and-7. The initiator caspases contain long

amino-terminal prodomains, which are not observed with the effector caspases. These long prodomains contain specific protein-protein interaction sites (DED: Death Effector Domain, CARD: CAspase Recruitment Domain), necessary for their association with specific activators (Boldin et al., 1996; Muzio et al., 1996; Hofman et al., 1997). This association allows for the attraction of more caspases and thus the induction of autoprocessing and activation of the specific caspase. The effector caspases are proteolytically activated by the initiator caspases and aid in the dismantlement of the cell by cleaving a great number of cellular proteins (Kumar and Colussi, 1999).

Currently, two main pathways regulate caspase activation in mammals. One pathway begins with the ligation of death receptors such as Fas/ tumour necrosis factor family of death receptors (TNF-R1). Subsequently, adapter molecules like Fas associated death domain (FADD) and TNF-R1 associated death domain protein (TRADD) are recruited which then generate a link between caspase-8 or –10 (group I procaspases) and the death receptors (Muzio et al., 1996; Medema et al., 1997). In the second pathway, a multitude of apoptotic stimuli provoke the release of cytochrome *c* from the mitochondria. Subsequently, Apaf-1, and pro-caspase-9 bind to cytochrome *c*, with the participation of dATP, which results in autocatalytic activation of caspase-9. Once activated, caspase-9 can then cleave and activate pro-caspase-3 directly, giving way to a cascade of caspase activation and enhanced apoptosis. Ultimately, caspase-8 and –9 have shown the ability to cleave and activate effector caspases –3, -6, and –7 (Takahashi et al., 1996; Li et al., 1997; Stennicke et al., 1998). (Figure 1)

**Figure 1: The activation of caspases through Fas/TNF-R1 and the mitochondrial pathways**

The Fas/TNF-R1 mechanism for triggering activation of caspases involves the recruitment of pro-caspase-8 to the activated membrane receptors through their association with adapter molecules, FADD/TRADD. The close association of the zymogens (pro-caspases) results in the processing of one another and subsequently downstream caspase activation. Caspase activation with the mitochondria involves the release of cytochrome c, that binds to Apaf-1 (apoptosis protease activating factor-1) and subsequently associates with pro-caspase-9 in the presence of dATP/ATP, resulting in the autocatalytic activation of caspase-9 and ultimately the cleavage of caspase-3 directly. Human IAPs, XIAP, HIAP1, HIAP2 directly inhibit caspases 3, 7 and 9. In addition, *survivin* can prevent apoptosis when caspases-3, -7, and –9 are overexpressed.

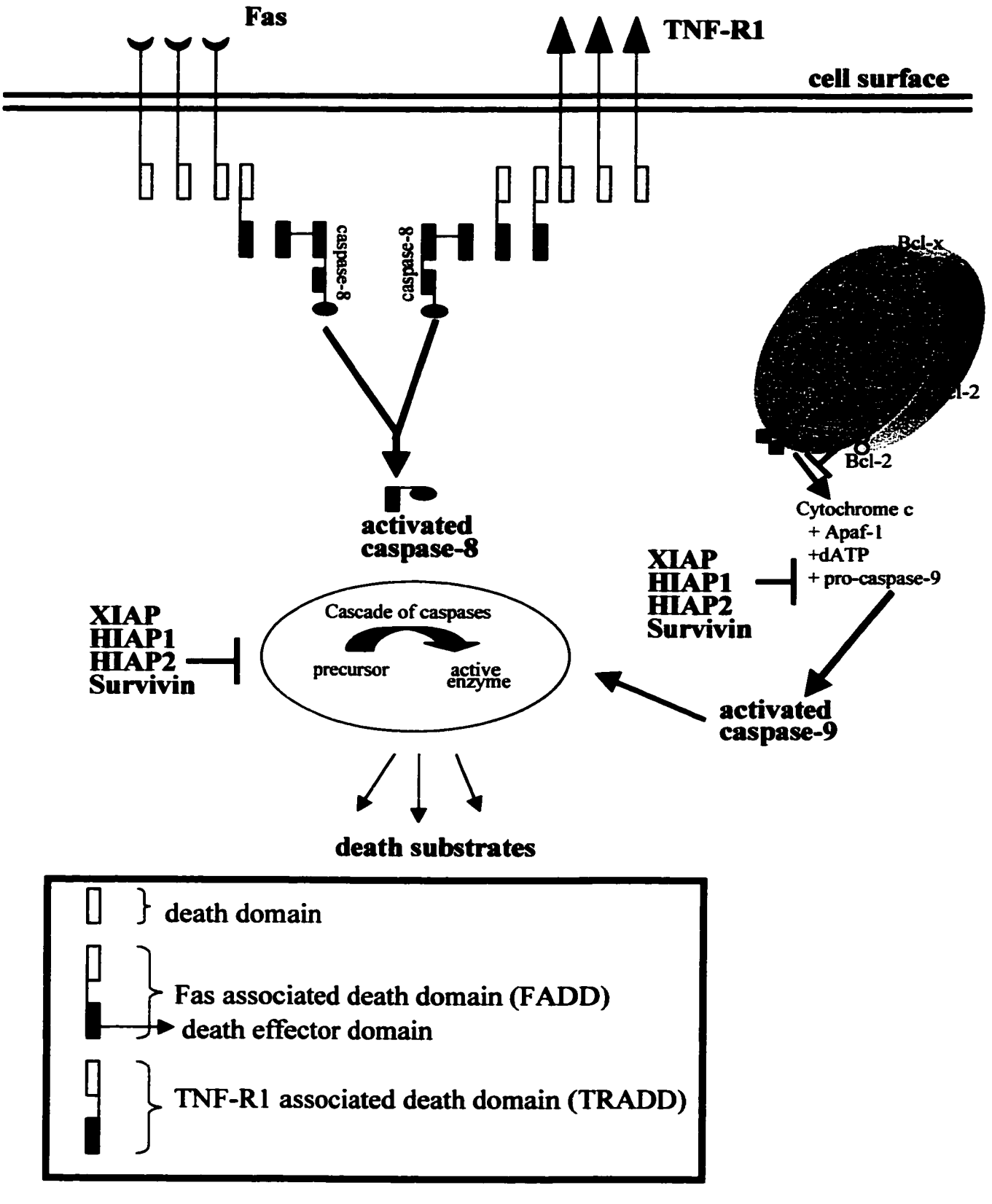
Fas
TNF-R1
cell surface
caspase-8
caspase-8
Bcl-x
Bcl-2
Cytochrome c
+ Apaf-1
+dATP
+ pro-caspase-9
activated
caspase-8
XIAP
HIAP1
HIAP2
Survivin
Cascade of caspases
precursor
active
enzyme
XIAP
HIAP1
HIAP2
Survivin
activated
caspase-9
death substrates
death domain
Fas associated death domain (FADD)
death effector domain
TNF-R1 associated death domain (TRADD)

#### 1.3.1.1 Caspase knockout mice

The exact role that each caspase plays in apoptosis is not clear and is complicated by the fact that they are often co-expressed in identical tissues. Furthermore, mammalian caspase "knockout" studies have revealed that certain caspases function in a spatio-temporal fashion during developmental cell death in the mouse. Mice deficient in caspase-9 and caspase-3 display very similar phenotypes. Caspase-9 is normally expressed during development and also in the adult mouse, and caspase 3 is observed in the embryonic mouse nervous system, more specifically, at E10.5 in the dorsal root ganglion, and ganglion complex (Mukasa et al., 1997; Hakem et al., 1998). Both knockout animals either die during development or shortly after birth. The majority of caspase-9 or -3 knockout mice develop profound hyperplasia in the brain caused by decreased developmental cell death in the proliferative neuroepithelium (Kuida et al., 1996, 1998; Woo et al., 1998; Hakem et al., 1998). In addition, at day10.5, caspase-9 knockout mice exhibit a defect in neural tube closure. Moreover, protrusions of the neuroepithelium in the retina are evident in caspase-3 knockout mice due to a decrease in apoptosis in this tissue (Kuida et al., 1996, 1998). These observations indicate that caspase-9 and caspase-3 do not compensate for the loss of the other during brain development and that caspase-3 is essential in normal eye development. Similar abnormalities observed in caspase-9 and -3 null mice are seen in mice lacking the caspase-9 activator, Apaf-1. These consist of brain hyperplasia, eye abnormalities, craniofacial abnormalities and reduced apoptosis of interdigital cells (Kuida et al., 1998; Hakem et al., 1998; Cecconi et al., 1998; Yoshida et al., 1998). This is *in vivo* confirmation that Apaf-1 belongs in the same signaling pathway as caspase-9 and –3, and

plays a nonredundant role in manipulating cell counts in brain and eye development. Additional abnormalities observed in Apaf-1 null mice and not in caspase-9 deficient mice would suggest that Apaf-1 may regulate other caspases other than caspase-9.

In contrast, caspase-8 deficient mice die between E11.5-E12.5 apparently due to abnormal heart development (Varfolomeev et al., 1998). Interestingly, mice deficient for FADD, which is a caspase-8 adaptor protein, are embryonic lethal at E12.5, with similar heart defects observed in caspase-8 null mice. Therefore, this would imply that the death receptor pathway involving caspase-8 and FADD is required during heart development (Yeh et al., 1998). The investigation of knockout mice of various caspases and their regulators has advanced our understanding of the apoptotic process during mammalian development. However, the role of other necessary components of the death machinery that promote or counter caspase activation, namely the pro- and anti-apoptotic members of the Bcl-2 family, are also being addressed.

### 1.3.2 Bcl-2 family of anti- and pro-apoptotic proteins

The Bcl-2 protein was initially discovered as a proto-oncogene in follicular B-cell lymphoma and subsequently was identified as the mammalian homologue to the apoptotic suppressor, *ced-9* in *C. elegans* (Tsujimoto et al., 1985; Hengartner and Horvitz, 1994; Thompson, 1995). Bcl-2 is principally located in the outer mitochondrial membrane, endoplasmic reticulum, and the nuclear membrane and inhibits apoptosis by blocking the release of cytochrome *c* from the mitochondria. Consequently, caspase activation and ultimately cell death are prevented (Krajewski et al., 1993; Kluck et al., 1997). With regards to the pro-apoptotic molecules, a substantial portion resides within cytosolic organelles prior to the induction of apoptosis (Hsu et al., 1997). Depending on

the cell type and death triggers, certain Bcl-2 family pro- and anti-apoptotic proteins have the ability to form either homo- or heterodimers and the ratio of either of these protein members can frequently decide the future of the cell (Oltvai et al., 1994; Yang and Korsmeyer, 1996). With respect to expression patterns, Bcl-2 protein is observed in a wide variety of developing murine tissues. Most notably, expression is seen in the neural tissues of the brain, dorsal root ganglia, developing lung, intestinal epithelium, kidney, and in the digital zones of the developing limb and no expression is observed in the liver after E12.5 (Novack and Korsmeyer; 1994). However, the overall levels of Bcl-2 expression decrease during the late stages of murine embryogenesis and is restricted to most lymphoid tissues in the adult mouse (Hockenbery et al., 1991). Bcl-2 expression is more prevalent in human fetal than in adult tissues implying the importance of this protein in normal homeostasis and morphogenesis of developing tissues (LeBrun et al., 1993).

To gain an understanding of the role of the Bcl-2 family of proteins *in vivo*, knockouts of some anti- and pro-apoptotic members have been developed. Mice deficient in Bcl-2, Bcl-$X_L$ or Bax have demonstrated that these proteins play distinct and nonredundant roles during development (Antonsson and Martinou, 2000). Intriguingly, Bcl-2 deficient mice were viable, without any recognized impairments of the CNS, although they usually died of renal failure a few months later (Veis et al., 1993). In contrast, Bcl-$X_L$ (anti-apoptotic) null mice displayed an increasingly severe phenotype in the developing CNS, not surviving past embryonic day 13. Most of the cell death in these knockouts is observed in the postmitotic immature neurons in the brain, spinal cord, and dorsal root ganglia (Motoyama et al., 1995). Mice deleted for Bax, a pro-apoptotic Bcl-2

family member, were viable, but infertile. The Bax knockout ovaries and testes showed excess accumulation of granulosa cells and spermatogonia respectively. Both tissue types had failed to undergo their normal developmental cell death (Knudson et al., 1995; Perez et al., 1997). Taken together, these results would imply that the different Bcl-2 members might have distinct roles in specific cell types. The observation that some members of the Bcl-2 family of knockout mice had maintained their viability would imply that other family members are possibly compensating for the lack of the specific protein. Nevertheless, other anti-apoptotic proteins could very well be aiding in the maintenance of developmental homeostasis and organogenesis.

### 1.3.3 IAPs (inhibitor of apoptosis proteins)

The inhibitor of apoptosis proteins (IAPs) are a family of very highly conserved apoptosis suppressing molecules initially discovered in the baculoviruses *Cydia pomonella* granulosis virus (CpGV) and *Orgyia pseudotsugata* nuclear polyhedrosis virus (OpMNPV). Homologues were subsequently found in many eukaryote species (Crook et al., 1993; Birnbaum et al., 1994; Liston et al., 1996; Deveraux and Reed, 1999). Members of the IAP family of proteins contain up to three copies of a novel Baculoviral Inhibitor of apoptosis Repeat (BIR) domain, spanning approximately 80 amino acids, containing conserved cysteine and histidine residues that represent a putative zinc binding fold (Deveraux and Reed, 1999). The majority of IAPs have an additional domain, a RING (Really Interesting New Gene, Freemount et al., 1991) zinc finger located in the carboxy terminus, that distinguishes it from other proteins.

The neuronal apoptosis inhibitory protein (NAIP) was the first human IAP to be identified as a partially deleted gene in patients with spinal muscular atrophy (SMA), an

autosomal recessive neuromuscular disorder marked by severe loss of motor neurons (Roy et al., 1995). To date, NAIP is the sole mammalian IAP to possess three BIR domains and no RING zinc finger (Figure 2). Despite the absence of this latter domain, NAIP is capable of suppressing apoptosis both *in vivo* and *in vitro* (Liston et al., 1996; Xu et al., 1997). Subsequently, four additional human IAPs were discovered, XIAP (X-linked IAP), HIAP-1 (Human IAP-1), HIAP-2 (Human IAP-2), and *survivin* (Duckett et al., 1996; Liston et al., 1996; Ambrosini et al., 1997) (Figure 2). XIAP, HIAP-1, and HIAP-2, as observed with the baculoviral IAPs, contain amino terminal BIR domains and a carboxy terminal RING zinc finger (Rothe et al., 1995; Liston et al., 1996; Duckett et al., 1996; Uren et al., 1996). However, the above mentioned IAPs contain three BIR domains as opposed to the two observed in the baculoviral IAPs. Additionally, HIAP-1 and HIAP-2 contain a CARD domain located between the BIR and RING zinc finger which is present in other proteins including caspases (Hofmann et al., 1997). This domain is longer in HIAP-1 and HIAP-2 than in the viral IAP proteins. Even though there is no evidence of protein-protein interactions attributable to this region of HIAP-1 and HIAP-2, it may be a target for caspase binding, since both proteins share homology in this domain. Lastly, *survivin* contains only one amino terminal BIR domain and is expressed in various cancers (Ambrosini et al., 1997), and embryonic or proliferating cells.

The mammalian IAPs (XIAP, HIAP-1 and HIAP-2, *survivin* and NAIP) can suppress cell death when induced by various apoptotic stimuli including TNF, Fas, growth factor/serum withdrawl, chemotherapeutic agents (etoposide, actinomycin D, taxol), menadione, and UV radiation (Duckett et al., 1996; Liston et al., 1996; Ambrosini

**Figure 2: Structural representation of BIR domain -containing proteins in various species**

Each inhibitor of apoptosis protein (IAP) member possesses at least one 80 amino acid BIR (baculoviral IAP repeat) domain (blue). The RING zinc finger (red) appears to be indispensable for baculoviral apoptotic inhibition, along with certain cellular IAPs, unlike NAIP, where it is unnecessary for suppression of apoptosis. Certain viral IAPs are not capable of inhibiting apoptosis in the presence of their BIR domains, for example, the African Swine Fever virus IAP (ASFIAP), *Chilo iridescent* Virus IAP (CiIAP), baculovirus *Autographa californica* Nuclear Polyhedrosis Virus IAP (AcIAP), as well as both *C. elegan* IAPs (CeIAP1 and CeIAP2). The CARD (caspase recruitment domain) motif (grey) is exclusively observed in proteins, like HIAP1 and HIAP2, known to be associated in apoptotic signalling.

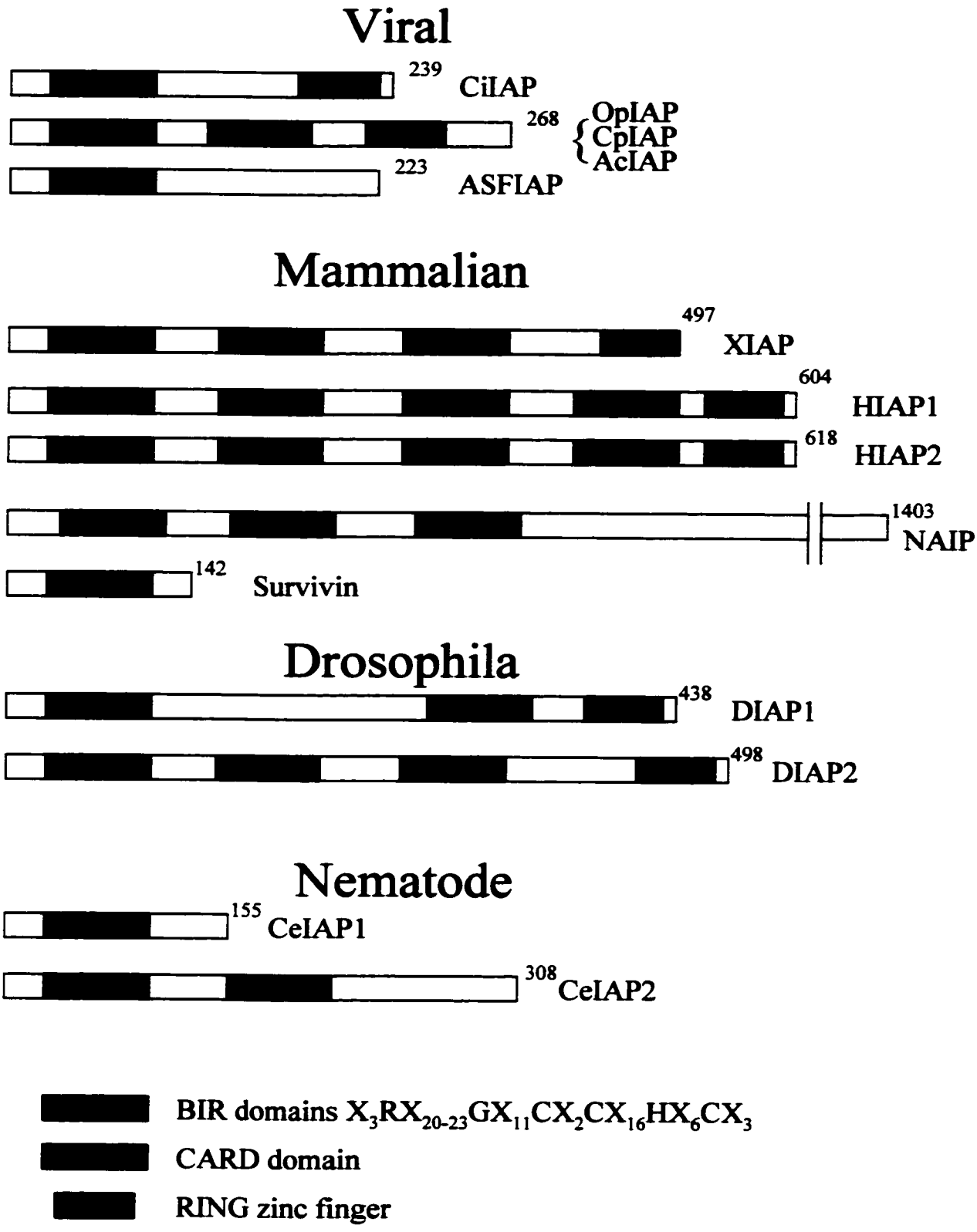
Viral
239
CiIAP
268
OpIAP
CpIAP
AcIAP
223
ASFIAP
Mammalian
497
XIAP
604
HIAP1
618
HIAP2
1403
NAIP
142
Survivin
Drosophila
438
DIAP1
498
DIAP2
Nematode
155
CeIAP1
308
CeIAP2
BIR domains $X_3RX_{20-23}GX_{11}CX_2CX_{16}HX_6CX_3$
CARD domain
RING zinc finger

et al., 1997; Li et al., 1998). In addition, these IAPs block a wider range of triggers in comparison to Bcl-2, suggesting that they operate downstream of the Bcl-2 family of proteins (La Casse et al., 1998). Moreover, they inhibit apoptosis induced by Bax, Bak and Bik, which are recognized for inducing cytochrome *c* release, yet the IAPs do not interfere with the release of cytochrome *c* induced by these Bcl-2 family members (Finucane et al., 1999). This places the mammalian IAPs downstream of certain Bcl-2 family proteins and cytochrome *c*. IAPs have been shown to suppress apoptosis through direct inhibition of caspases (Roy et al., 1997; Deveraux et al., 1998; Tamm et al., 1998;). More specifically, XIAP, HIAP-1, and HIAP-2 were each shown to bind to and potently inhibit activated caspase-3 and -7, as well as the activation of pro-caspase-9 *in vitro* (Figure 1). However, this was not observed with caspases-1, -6, -8, -10 or the *C. elegans* caspase, *ced-3* (Deveraux et al., 1997, 1998; Roy et al., 1997). Since these IAPs are able to bind to and inhibit caspase-3, the effector caspase in the cytochrome *c*/Apaf-1 induced cascade, it is possible that they also hinder the amplification loop that involves the additional cleavage and activation of pro-caspase-9 by activated caspase-3 (Srinivasula et al., 1998). An additional IAP, *survivin,* is capable of suppressing cell death induced by overexpression of the caspase-3, -7 and -9 (Tamm et al., 1998). The portion of the IAPs that are both sufficient and indispensable for caspase inhibition and apoptosis are the BIR domains (Deveraux et al., 1997; Roy et al., 1997). *Survivin* contains only one BIR domain, however it is sufficient to bind caspases and forestall cell death (Tamm et al., 1998). Moreover, of all the human IAPs to date, XIAP appears to be the most potent inhibitor of caspases, a property that is most evident with its second BIR domain (BIR 2) (Takahashi et al., 1998).

Caspase inhibition is not the sole mechanism by which IAPs suppress cell death. Recently, it has been shown that XIAP, HIAP-1 and HIAP-2 can inhibit apoptosis through their associations involving the transcription factor NF-κB. Upon TNFα ligation, TNFR-1 trimerization results in NF-κB translocation to the nucleus where it activates the expression of several anti-apoptotic proteins. These include, HIAP-1, HIAP-2, and XIAP, cA20 and certain Bcl-2 family members (Liston et al., 1997; Deveraux and Reed, 1999). Moreover, HIAP-2 can indirectly (through its RING domain) activate NF-κB, and its protection of Jurkat T-cells from TNFα mediated apoptosis is NF-κB dependent (Chu et al., 1997). Furthermore, this activation of IAP expression, that is, an increase in HIAP-1, HIAP-2, and XIAP expression was observed when primary endothelial cells were stimulated with TNFα. This function is likely to be downstream of NF-κB, since overexpression of IkB (inhibitor of NF-κB), which results in supression of NF-κB activation, also prevents IAP induction (Stehlik et al., 1998). In contrast to primary endothelial cells, HIAP-1 expression levels in Jurkat cells were invariable and did not appear to be regulated by NF-κB (Chu et al., 1997). These data suggest that the expression of IAPs vary from cell to cell, and as a result, so does their anti-apoptotic participation.

The *survivin* protein was found to associate with the microtubules of the mitotic spindle at the beginning of mitosis, through its carboxy terminal coiled coil and BIR domains. Moreover, disruption of this connection abrogates *survivin's* anti-apoptotic activity (Li et al., 1998).

Currently, little is known about specific IAP functions during development. However, *in vivo* expression patterns for survivin have been characterized during mouse

and human embryogensis. During early mouse development *survivin* appears more prominent and ubiquitous than at later stages. The distribution of *survivin* is distinct from that of Bcl-2 in that *survivin* is not seen in adrenal gland, retina, trophoblast, whereas Bcl-2 is. Conversely, *survivin* is seen in epidermis, and in approximately 20% of liver cells, while Bcl-2 expression is not observed in the epidermis or the liver (LeBrun et al., 1993). During E15-21, *survivin* expression is confined to apoptotic regulated areas, including lung, dorsal root ganglion neurons, hypophysis, spinal cord, and the choroid plexus (Adida et al., 1998). *Survivin*, like Bcl-2, appears to play a role during morphogenesis, by affecting the balance of survival factors within cells of developing tissues. In contrast, in normal adult tissues, *survivin* is undetectable, although it is abundantly expressed in most of the common human cancers (Ambrosini et al., 1997). Thus, cell survival and proliferation rely on a balancing act that *survivin* and the additional IAPs must perform to ensure equilibrium within the organism (Adida et al., 1998).

### 1.3.4 *XIAP*

The *xiap* (X-linked IAP) gene was identified using IAP sequences from *Cydia pomonella*, and is located on the human X chromosome at Xq24-25 (Liston et al., 1996). This region is predisposed to immune system disorders, such as the X-linked lymphoproliferative disorder. However, material from the few patients available with the affliction appear to have no noticeable deletions in the *xiap* gene (Liston et al., 1997). The *xiap* gene spans approximately 30 kb and contains seven exons encoding 9 kb of mRNA that is translated into a 55 kDa protein (Liston et al., 1996). All three BIR domains reside within a single exon, which is also observed for the RING zinc finger (Liston et al., 1997). The *xiap* transcript contains a particularly long 5' untranslated

region (UTR), (greater than 1.6 kb) with presumed complex secondary structures and several possible translation initiation sites upstream of the actual initiation codon. Therefore, it is assumed that problems would be encountered if the typical ribosome scanning method of translation initiation were utilized. Characterization of the 5' UTR nucleotide sequence of *xiap* revealed a unique Internal Ribosome Entry Site (IRES) element (Holčik et al., 1999). Furthermore, it is now evident that the translation of *xiap* is mediated by the IRES element found within 162 nucleotides upstream of the initiation codon *in vitro*. Significantly, IRES mediated translation of *xiap* is resistant to the reduction of protein synthesis, which normally precedes apoptosis (Holčik et al., 1999).

#### 1.3.4.1 XIAP expression

Northern blot analysis using poly $(A)^+$ RNAs from several types of human adult and fetal tissues revealed a 9 kb *xiap* message. Expression of *xiap* was observed prominently in pancreas, kidney, skeletal muscle, spleen, thymus, prostate, testis, ovary, small intestine, and colon and at somewhat lower levels in the liver, lung, placenta, brain, heart and peripheral blood leukocytes (Liston et al., 1996).

*In vivo* data showed that the loss of rat CA1 hippocampal neurons following transient forebrain ischemia was preceded by a distinct increase in active caspase-3 protein, signifying apoptosis (Xu et al., 1999). However, adenoviral-mediated overexpression of XIAP has been shown to reduce the loss of these neurons and at the same time prevent the accumulation of active caspase-3. This suggests that caspase-3 activation is an important event in neuronal cell loss in forebrain ischemia and that *xiap* gene therapy can prevent this neurodegeneration (Xu et al., 1999).

In *xenopus* embryos it has been shown that overexpression of XIAP enhances early ventral mesoderm formation in a TAB1-TAK1 dependent manner (Yamaguchi et al., 1999). TAK1 is a member of the MAP kinase kinase kinase family and TAB1 is its activator. XIAP was found to associate with the TAB1 protein through its amino terminus, as well as with the BMP type I receptor (BMP: member of the TGF-β superfamily) through its RING finger motif. This interaction is also observed with *Drosophila* DIAP-1, which interacts with Dpp type I receptor through the RING finger (Oeda et al., 1998). It has also been shown that TAK1 can induce cell death and that this can be blocked by overexpression of XIAP in *xenopus* embryos (Yamaguchi et al., 1999). These results suggests that XIAP inhibits apoptosis during early *xenopus* development and neutralizes TAK1 activity by associating with caspases and TAB1, respectively.

#### 1.3.4.2 *Miap3*

The murine homolog of *xiap*, *miap3* (murine IAP3), is mapped to mouse chromosome X region A3-A5, which is syntenic to the human chromosome Xq25 containing *xiap* (Rajcan-Separovic et al., 1996). *Miap3*, like *xiap*, contains three BIR domains and a RING zinc finger domain in the amino and carboxy termini, respectively. It is composed of six exons, spanning approximately 20 kb and has a coding region of 1.5 kb. *Miap3* and *xiap* are 94% identical at the amino acid level and both code for a 55 kDa polypeptide. *Miap3* also shares 87% DNA homology with *xiap*. The 5' and 3' UTRs of *miap3* are greater than 5.5 kb and 1.6 kb, respectively and show less than sixty percent identity with *xiap's* UTRs, implying that these areas contain species-specific regulatory elements (Farahani et al., 1997). Also, the first exon harbors the first two BIR domains, and part of the third BIR domain. The rest of BIR three is found in the second and third

*miap3* exons. Total RNA derived from various adult CD-1 mouse tissues was used for Northern blot analysis, and had revealed an 8 kb band in all adult tissues examined, with brain and lung having more prominent expression. *In vitro* studies demonstrate that *miap3* protein is localized cytoplasmically (Farahani et al., 1997).

**1.4 Thesis objective**

XIAP, clearly protects various cell types against apoptosis induced by a wide variety of triggers, a property which is in contrast to the more limited scope of the Bcl-2 family of anti-apoptotic proteins (LaCasse et al., 1998). This implies that XIAP can function downstream of the Bcl-2 family of proteins. Moreover, XIAP appears to be a potent and direct inhibitor of caspases-3, -7, and -9 (Deveraux and Reed, 1999).

Due to the fact that XIAP has only recently been cloned, there are few data at present concerning its expression and its *in vivo* functions. The overall pattern of expression of the human XIAP gene has been examined by Northern blot analysis which revealed a ubiquitous pattern of XIAP message in various adult and fetal tissues (Liston et al., 1996). On the basis of these discoveries, we postulated that the XIAP gene product is possibly required for development, function and maintenance of various tissue systems.

The objective of this project was to analyze spatial and temporal patterns of expression of the XIAP gene during murine embryogenesis and correlate it with the cell death events that occur during development using both radioactive and non-radioactive *in situ* hybridization. In addition, using immunofluorescence studies with a polyclonal rat version of XIAP antibody, we sought to determine whether XIAP protein is co-localized with XIAP message. Therefore, by studying the expression of this apoptotic inhibitor in

mouse development, a role for XIAP during development may be elucidated.

## 2. Materials and Methods

### 2.1 PCR analysis of *miap3* during embryogenesis

Commercially available cDNA (Clontech, 0.3 ng) isolated from whole embryo at embryonic day (E)7 and E11 was used in a 25 µl reaction each containing 1X PCR buffer (Gibco/BRL), 3mM $MgCl_2$(Gibco/BRL), 0.8mM each dNTP (Gibco/BRL), 10-20 units of Taq polymerase (Gibco/BRL) and 50ng of both upstream and downstream primers. The upstream (5'-TCTGGTGTGAGTTCTGATAGG-3') and downstream (5' GGGAAGAACTGCTGAAAAAGAATTCTA-3') primers consisted of sequence from the first and fourth exons respectively. Amplification conditions were as follows: 1 cycle at 94°C/5 min. 35 cycles at 94°C/30 seconds, 57°C/1 min, 72°C/1 min and 1 cycle at 72°C/10 min was performed in a Perkin Elmer ABI 9600. PCR products were electrophoresed on a 1.5% agarose gel and visualized by ethidium bromide staining (0.5 µg/ml). β-actin served as a loading control for day 7 and 11 *miap3* cDNA. A 250 bp product was amplified using the β-actin primers (upstream: 5'-GGAGCAATGATCTTGATCTTC-3', downstream: 5' CCTTCCTGGGCATGGAGTCCT-3').

### 2.2 Whole-mount *in situ* hybridization

#### 2.2.1 Preparation of plasmids and DIG-labeled riboprobes

Single-stranded *miap3* antisense and sense riboprobes were synthesized as run-off transcripts from linearized plasmids using a bacteriophage T7 RNA polymerase. *Miap3* cDNA, 5' UTR and 3' UTR were provided by Martin Holčik. The 485 bp probe fragment is contained in the region between BIR1 & 2 and the 339 bp probe fragment between BIR3 and the RING zinc finger of *miap3* (Figure 3). Both probes were generated by PCR

**Figure 3: Location of *miap3* riboprobes used for *in situ* hybridization**

This schematic illustrates the three highly conserved BIR domains (blue) towards the 5' UTR (untranslated region) and the RING zinc finger motif (red) close to the 3' UTR. For whole-mount and radioactive *in situ* hybridization, both 485 bp and 339 bp riboprobes were used. The 485 bp probe originates from the area between BIR1 and BIR2, whereas the 339 bp riboprobe is shown between BIR3 and the RING zinc finger motif. These probes were amplified by PCR from *miap3* full length cDNA and were cloned into pCDNA3 expression vector. The 485 bp and 339 bp antisense products were subcloned into pGem –7ZF (+/-) and the sense products were subcloned into pcDNA3 downstream of the T7 promoter.

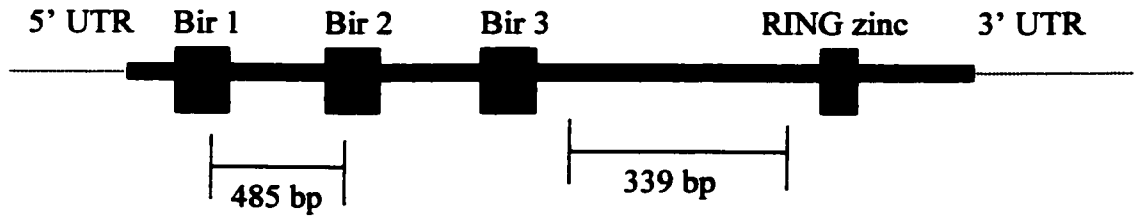
5' UTR
Bir 1
Bir 2
Bir 3
RING zinc
3' UTR
485 bp
339 bp

using two sets of primers that were specifically designed with Not I restricition sites incorporated into the 5' and 3' ends of both primers of each set. In a 25µl PCR reaction, 40 ng of *miap3* cDNA was used with the same concentration of reagents and primers as in section 2.1. The upstream (5'-GGGGGCGGCCGCGCGCGAGCTGGGTTTCTTT-3') and downstream (5'-GGGGGCGGCCGCTTTTTCAGTTTTCCCCC-3') primers had generated the 485 bp fragment and these upstream (5'-GGGGGCGGCCGCGGGGCAAGAATATATAAAT-3') and downstream (5'-GGGGGCGGCCGCTCCTCTTGTAGGCGCC-3') primers had generated the 339 bp fragment. Amplification conditions were as follows: 1 cycle at 94°C/10 min, 35 cycles at 96°C/1 min, 48°C/1 min 30 sec, 72°C/1 min and 72°C/10 min. Both products were digested with Not I, and subcloned into the Not I site of the pcDNA3 expression vector. All clones were in the forward orientation, therefore, to obtain an antisense orientation, the 485 and 339 bp products were excised from pcDNA3 (Invitrogen) with BamH I and Xba I and subcloned into the Xba I and BamH I sites of the pGEM -7Zf (+/-) (Invitrogen) expression vector. They were designated pGEM 485 antisense and pGEM 339 antisense. To generate templates, antisense and sense vectors were linearized with BamH I and Xho I respectively. Next, phenol chloroform (1:1) extraction and ethanol precipitation were used to purify the linearized plasmid DNA. The templates were then resuspended in TE buffer (10 mM tris-HCl, 1 mM EDTA pH 8.0).

Single-stranded RNA probes were labeled by *in vitro* transcription in the presence of DIG-11-UTP according to the instructions provided by Boehringer Mannheim. Briefly, the following were mixed in order at room temperature: 15 µl of sterile autoclaved distilled water, 3 µl of 10X DIG RNA nucleotide mix ( 10 mM each of ATP, CTP, and

GTP; 6.5 mM UTP; 3.5 mM DIG-11-UTP; pH 7.5, Boehringer Mannheim), 3 µl of 10X transcription buffer (400 mM tris-HCl pH 8.0, 60 mM $MgCl_2$, 100 mM DTT, 20 mM spermidine, Boehringer Mannheim), 1 µg of linear template, 2 µl of RNasin (Boehringer Mannheim 100 U/µl) and 2 µl of T7 RNA polymerase (Boehringer Mannheim10 U/µl). This mixture was incubated for 2 h at 37°C. After the 2 h incubation, 1 ul of probe ( +4 µl of $ddH_2O$ + 1 µl of loading buffer) was run on a 1% agarose gel made in TAE containing 0.5 µg/ml of ethidium bromide to estimate the amount of RNA synthesized (to minimize the risk of RNase contamination, the gel box was treated with 0.1 M NaOH for 30 min and then washed with tap water followed by $ddH_2O$). The RNA bands were approximately 10 times more abundant than the plasmid band, indicating that approximately 10 µg of riboprobe was synthesized. Next, 2 µl of DNase I (ribonuclease-free) was added to the probes and incubated at 37°C for 15 min, to remove the DNA template. The probes were precipitated in100 µl of TE, 10 µl of 4 M LiCl and 300 µl of 100% ethanol at -20°C overnight. The following day, probes were centrifuged at 14,000 rpm for 10 min, washed twice with cold 70% ethanol and centrifuged at 14,000 rpm for 10 min. The pellets were air dried and dissolved in 100 µl of TE buffer to yield a final concentration of 0.1 µg/µl. The DIG-labeled riboprobes were stored at -20°C until their use.

2.2.2 Quantification of DIG-labeled probes

To estimate the yield of DIG-labeling, dilutions of the DIG-labeled riboprobes were spotted on quantification teststrips (Boehringer Mannheim). The intensities were compared to a series of DIG-labeled DNA standards. DIG-High Prime reaction yields

approximately 40 μg/ml of DIG-labeled DNA. Subsequently, the riboprobe teststrips were compared to the DIG control teststrips to determine the approximate incorporation of DIG-UTP in each of the riboprobes.

2.2.3 Preparation of mouse embryos

Mouse embryos were obtained from pregnant CD-1 mice. (ordered timed pregnancies, Charles River). The day the vaginal plug appeared was designated E0. Pregnant mice were euthanized by $CO_2$ and embryos were removed at various times between E9.5 to E13. Mouse embryos were dissected free of extra embryonic membranes in cold 1X PBS and transferred into 4%PFA/0.2% gluteraldehyde in PBS and stored at 4°C overnight. Procedures for mRNA detection from this point forward were performed under RNase-free conditions using RNase-free solutions, vials and containers.

2.2.4 Fixation and pretreatment of E9.5 to E12.5 embryos

Following overnight fixation, embryos were washed twice in PBT for 5 min at 4°C. Embryos were dehydrated twice by successive washes of 30%, 50%, 70%, 80%, 90%, 95% MeOH/PBT for 10 min at 37°C and then twice for 10 min in 100% MeOH. Embryos older than E10 were pierced just below the back of the head in order to prevent possible trapping of riboprobes and antibodies that could cause non-specific signals. At the same time, E12 embryos were hemi-sectioned sagittally to allow the probe better access to the target message. Therefore, a clearer pattern of expression could be visualized in many regions of the embryo. Embryos were then rehydrated in 75%, 50% and 25% MeOH/PBT for 10 min each and washed twice for 5 min in PBT at room temperature. E9.5 embryos were bleached with 6% $H_2O_2$ in PBT for 10 min and older embryos were bleached for 1 h. Embryos were then washed three times for 5 min

followed by digestion with 10 μg/ml of proteinase K (Gibco/BRL) in PBT at 37°C. E9.5 and older embryos were digested for 5 and 30 min., respectively, followed by three 5 min washes in PBT. Embryos were postfixed at 37°C for 20 min with 4% PFA/0.2% gluteraldehyde in PBT, then washed three times in PBT.

2.2.5 Hybridization of E9.5 to E12.5 embryos

Fixed embryos were incubated for 1 h at 58°C in prehybridization mix (50% deionized formamide, 5X SSC pH 4.5, 1% SDS, 50 μg/ml heparin). Fresh prehybridization solution containing 50 μg /ml of tRNA was added to the embryos and incubated for another hour at 58°C. The prehybridization solution was then replaced with 0.5 ml of hybridization solution (0.5 ml of prehyb mix + 2.5 μl tRNA + 0.5 μg of DIG antisense/sense probe) per vial of embryos which were continuously rotated overnight at 58°C.

2.2.6 Posthybridization washes and blocking of embryonic tissues

All the incubations and washes were carried out with gentle rocking. The following day, the hybridization solution was removed and the embryos were washed twice in solution 1 (50% deionized formamide, 5X SSC pH 4.5, 1% SDS) for 30 min at 60°C. A 1:1 mix of solution 1/solution 2 ( 0.5 M NaCl, 10 mM tris-HCl pH 7.5, 0.1% Tween-20) was performed for 10 min at 60°C and then with solution 2 three times for 5 min at 37°C. The embryos were treated twice in solution 2 containing 100 μg/ml of RNase A for 30 min at 37°C and then washed in solution 2 for 5 min at 37°C. In addition, the samples were washed twice in solution 3 (50% deionized formamide, 2X SSC pH 4.5) for 30 min at 60°C and three times for 5 min each in PBT. Mouse embryos were then incubated in blocking solution {10% sheep serum (heat-inactivated at 70°C for 30 min)

and 2% BSA in PBT} for 2-3 h at 37°C. The blocking solution was replaced with anti-DIG-AP Fab fragment solution (which was preabsorbed with mouse embryo powder for 3 h at 4°C, section 1.2.8) and incubated at 4°C overnight.

2.2.7 Post-antibody washes and immunological detection

The following day, the preabsorbed DIG antibody solution was removed and the embryos were transferred into 15 ml tubes and washed three times for 5 min in PBT at room temperature. In addition, fresh PBT was added to the embryos every 4 h, followed by an overnight wash in PBT with gentle rocking. The next day, embryos were washed twice in NTMT buffer (100 mM NaCl, 100 mM tris-HCl pH 9.5, 50 mM $MgCl_2$, 0.1% Tween-20 and 2 mM levamisole) for 10 min, followed by a 30 min wash in NTMT. The embryos were transferred to a 6 well plate and each well was submerged in 2 ml of 0.150 mg/ml NBT/ 0.175 mg/ml BCIP (Boehringer Mannheim) in NTMT for 7 h at room temperature. The plate was covered with aluminum foil and gently rocked until the desired signal intensity was achieved. The embryos were washed in PBT to stop any further colour development. Embryos were viewed the next day using an Olympus DF Planaro dissecting microscope and photographs were captured with an Olympus SC35 Type 12 camera.

2.2.8 Preparation of embryonic powder and preabsorption of anti-DIG-antibody

Approximately 50 mouse embryos from E12 were used to prepare 1 ml of mouse embryo powder. A PT 1200C polytron (Kinematica) was used to homogenize the mouse embryos in a minute volume of PBS. Four volumes of ice-cold acetone were mixed very well with the homogenized embryos and incubated on ice for 30 min. Subsequently, the mixture was spun at 10,000 rpm for 10 min at 4°C. The pellet was washed once more

with acetone and spun again under the same conditions. The pellet was spread out onto a clean filter paper and ground into a fine powder, where it was left to air dry. It was then stored in an Eppendorf tube at 4°C.

Anti-DIG-antibody was preabsorded with mouse embryo powder as follows: for every 3 mg of embryo powder used, 0.5 ml of 10% sheep serum, 2% BSA in PBT and 1 µl of anti-DIG-AP Fab fragment (Boehringer Mannheim) was added. This solution was rocked gently for 3 h at 4°C and then spun at 14,000 rpm for 10 min at 4°C. The supernatant was removed and diluted to 2 ml with 10% sheep serum, 2% BSA in PBT, resulting in a 1:2000 antibody dilution.

2.2.9 Controls for whole-mount *in situ* hybridization

Sense probes served as negative controls in all of the experiments. As a positive control, *myogenin* was used as described in Sassoon et al., (1989). pcDNA3 *myogenin* (+) and (-) (a gift from Chris Storbeck) were obtained by cloning a 450 bp EcoR I fragment from the 3' end of the myogenin coding region into the EcoR I multiple cloning site of pcDNA3 expression vector in the antisense and sense orientations. The antisense and sense myogenin vectors were linearized with Xho I (downstream of the T7 RNA polymerase promoter and myogenin fragment) and *in vitro* transcribed as described in section 2.2.1

## 2.3 Radioactive *in situ* hybridization

2.3.1 Preparation of mouse embryo sections

E9.5 to E16 embryos were prepared as described for whole-mount *in situ*, with the following exceptions. Embryos of E9.5 to E12 were placed in formalin overnight and embryos older than E12 were preserved for an additional 2-3 days. Embryos were then

processed in the solutions and times indicated: PBS for 30 min at 4°C, 0.85% saline solution for 30 min at 4°C, (next steps were performed at 25°C) 50% ETOH in 0.425% saline 2X for 15 min, 70% ETOH for 30 min, 85% ETOH for 30 min, 95% ETOH for 30 min, 100% ETOH 2X for 30 min, xylene 2X for 30 min, and a 1:1 solution of xylene:melted paraplast at 60°C for 45 min. The embryos were transferred through paraplast 3X for 20 min each at 60°C, then embedded and oriented in plastic moulds, preheated to 60°C, cooled and stored at 4°C. Mouse embryo sections were cut with a microtome (Zeiss) into 6 μm ribbons which were floated on a bath of distilled water at 50°C until the creases disappeared. The sections were collected on silane coated slides (SIGMA), dried at 37°C overnight and stored desiccated at 4°C.

2.3.2 Preparation of plasmids and $^{33}$P- labeled riboprobes

To detect *miap3* mRNA, both the 485 bp and 339 bp antisense and sense templates were used for the synthesis of the riboprobes (Figure 3.). The antisense and sense 485 bp and 339 bp riboprobes were prepared as indicated for whole-mount *in situ* (section 2.2.1), except $^{33}$P-UTP was used instead of DIG-11-UTP. The templates were *in vitro* transcribed according to manufacturer's instructions (MAXIscript, Ambion). Briefly, RNase-free water was added to achieve a total volume of 20 μl, 2 μl of 10X transcription buffer (containing DTT), 0.5 mM ATP, 0.5 mM CTP, 0.5 mM GTP, 3.125 μM $^{33}$P-labeled UTP, 1 μg of linearized DNA template and 20 units of T7 RNA polymerase containing 10 units of RNase inhibitor. The reactions were incubated for 1 h at 37°C. To remove template DNA, 2 units of RNase-free DNase I was added to each reaction and incubated for an additional 15 min at 37°C. Unincorporated nucleotides were removed by size exclusion chromatography on RNase-free Sephadex™ G50 spin

columns (SIGMA). To determine the specific activity of each probe, 1 µl from a 1:10 dilution of probe was added to 400 µl of liquid scintillation fluid and subjected to scintillation counting (1450 Microbeto PLUS , WALLAC). *Myogenin* served as a positive control for the *in situ* hybridization experiments.

2.3.3 $^{33}$P *in situ* hybridization

Embryo sections were deparaffinized in xylene 2X for10 min and rehydrated through a series of ethanols, 2X 100% for 1 min each, and 1X 95/85/70/50/30% for 1 min each. They were rinsed in 0.9% saline for 5 min and then in PBS for 5 min. The sections were postfixed in freshly prepared and filtered 4% PFA in PBS for 20 min. The slides were washed twice in PBS for 5 min each and were treated with proteinase K (Gibco/BRL, 20 µg/ml) in 50mM tris-HCl pH 7.2 and 5mM EDTA pH 7.2 for 8 min. Following this, the slides were washed in PBS for 5 min before they were postfixed in 4% PFA in PBS for another 20 min. The slides were then dipped in distilled water before being acetylated in 0.1 M triethanolamine containing 0.25% acetic anhydride in 0.9% NaCl for 10 min. Subsequently, the slides were rinsed in PBS and 0.9% saline for 5 min each. The sections were dehydrated through a series of 30/50/70/85/95 and 100% ethanols for 1 min each and the slides were air dried for 1 h at room temperature. Hybridization solution ( 200 µl of 50% formamide, 0.3 M NaCl, 20 mM tris-HCl pH 7.4, 5 mM EDTA pH 7.4, 10 mM $NaPO_4$ pH 8.0, 1X Denhardt's, 10% Dextran sulfate) was added to each slide, a coverslip was then applied and embryo sections were incubated in a humidified chamber at 58°C overnight. Each probe contained 2 x $10^7$ cpm/ ml of hybridization solution.

The following day the coverslips were gently removed in 5X SSC/10 mM DTT at 50°C. The slides were then washed in 50% formamide, 2X SSC, 100 mM DTT at 60°C for 30 min, rinsed briefly in NTE buffer ( 0.5 M NaCl, 10 mM tris-HCl pH 8.0, 5 mM EDTA pH 8.0) and then in NTE buffer containing RNase A (20 μg/ml Boehringer Mannheim) for 40 min at 37°C. Slides were then washed in 2X SSC and 0.1X SSC for 15 min each at room temperature. They were then dehydrated through a series of ethanol's: 30/60/80/95% containing 0.3 M ammonium acetate and 2X 100% ethanol for approximately 1 min each before being air dried.

Processing involved dipping the slides into photographic emulsion prewarmed to 42°C (Kodak NTB-2 autoradiographic emulsion) in a darkroom. The slides were air dried for 2 h before they were placed horizontally in a light-tight box containing desiccant. The box of slides was exposed for 3 weeks at 4°C before development. Prior to development, the box of slides were removed from the 4°C and warmed to room temperature. In a dark room, the slides were transferred through a 1:1 dilution of Kodak D19 developer and water for 5 min, distilled water for 10 sec, Kodak fixer for 5 min and distilled water for 5 min, all at 16°C. In addition, the slides were stained with a 1:50 dilution of 0.02% toluidine blue for 5 min, dehydrated in a series of ethanols: 50/75/95/100%, and immersed in xylene for several minutes prior to mounting the sections with Permount (SIGMA). Images were analyzed using both light and dark field optics with a Zeiss Axiophot microscope connected to a Sony PowerHAND video camera, using Northern Eclipse 4.0 software. An Olympus DF Planaro dissecting microscope was used to capture the whole embryo section under darkfield illumination and photographs were captured with an Olympus SC35 Type 12 camera.

**2.4 Protein preparation and Western blot analysis**

For tissue extracts, adult CD-1 mouse tissues and whole CD-1 mouse embryos from E9 to E13 were homogenized in a buffer consisting of 10 mM tris-HCl pH 8.0, 150 mM NaCl, 2 mM $MgCl_2$, 1 mM PMSF and 10 μg/ml aprotinin. The lysates were adjusted to 2% SDS and boiled for 20 min before being centrifuged twice at 14,000 rpm for 10 min. Total protein concentration was determined using a Micro BCA protein assay kit (Pierce) according to the manufacturer's instructions. For western blot analysis, 25-30 μg of total tissue protein was lysed in 3X reducing SDS sample buffer (1/10 volume of 30X reducing agent: 1.25 mM DTT was added to 1 volume of 3X SDS sample buffer: 187.5 mM tris-HCl, pH 6.8, 6% SDS, 30% glycerol and 0.03% bromophenol blue, New England Biolabs) and boiled for 5 min, prior to being resolved on a 10% SDS-PAGE gel (Sambrook *et al.*, 1989) using a Biorad mini-Protean II apparatus system. Proteins were transferred to polyvinylidene difluoride membranes (PVDF, Immobilon-P) using the Hoeffer apparatus. Transfer efficiency was estimated by staining the membranes with 0.2% Ponceau S (Sigma). The membranes were blocked with 5% skim milk powder in PBS/0.05% NP40 overnight at 4°C. Tissue blots were incubated for 1 h at room temperature using a 1:2000 dilution of RIAP3 antibody (stock at 1.7 mg/ml provided by Apoptogen). To control for equal loading of protein, a mouse α-actin monoclonal antibody (SIGMA) was used at a 1:5000 dilution. The primary antibodies were detected using horse radish peroxidase-labeled goat anti-rabbit or anti-mouse IgG (secondary) antibodies at 1:3000 dilution as recommended by the manufacturer (Amersham). Subsequently, the membranes were washed in PBS/0.05% NP40 4X/15 min at room temperature. The binding of the primary antibody was visualized by enhanced

chemiluminescence using ECL reagents according to the manufacturer's specifications (Amersham). Signals were observed after a 20 min exposure to Kodak X-OMAT AR film. Scanning of the audioradiographs was performed with the VistaScanner program.

### 2.5 Immunofluorescence and immunohistochemistry procedures and analysis of MIAP3

CD-1 mouse embryos from E10 to E16.5 were prepared as described above (section 1.4.1). Serial sections were deparaffinized and rehydrated through a series of graded alcohols. After a rinse in water for 30 s, (sections to be used for immunohistochemistry were immersed in 3% $H_2O_2$ in PBS) sections were placed in citric acid buffer pH 6.0 and were boiled over a 10 min period with 30 s pauses immediately after boiling was achieved. Following a rinse in PBS and a wash in PBS for 2 min, the sections were incubated with 10% normal sheep or goat serum for 1 h at room temperature. Sections were incubated with a 1:100 dilution of anti-RIAP3 antibody or preimmune serum for 12-14 h at 4°C. Following the incubation with primary antisera, sections were rinsed in PBS for 5 min and MIAP3 was localized by incubation with either CY3-labeled sheep anti-rabbit secondary antibody (SIGMA) or (Alexa 488) fluorescein-labeled goat anti-rabbit secondary antibody (Molecular Probes). For immunohistochemistry, biotinylated goat anti-rabbit IgG was used as the secondary antisera in conjunction with avidin reagent, ExtrAvidin-Peroxidase (Sigma). DAB (3,3'Diaminobenzidine Tetrahydrochloride, SIGMA) was the precipitating substrate used for the detection of peroxidase activity. The sections were examined and photographed using a Zeiss fluorescence microscope.

## 2.6 Large scale preparation of plasmid DNA

Plasmid DNA was isolated using an alkaline extraction procedure (Birnboim and Doly 1979). Briefly, the plasmid of interest was grown in 200 ml of LB media (1% Bacto-tryptone, 0.5% yeast extract and 1% NaCl) containing 50 μg/ml of ampicilin and 10% glucose for 12 to16 hr in a 37°C shaker incubator. Once the cultures were harvested, the DNA was purified from the cell extract, concentrated by ethanol precipitation and resuspended in 2.4 ml of TE buffer. To prepare the DNA for CsCl density gradient centrifugation, 2.75 g of CsCl (Gibco/BRL) and 260 μl of ethidium bromide (10 mg/ml) were added to the samples. The samples were placed into ultracentrifuge tubes (Beckman) and were centrifuged at 80,000 rpm for 14 to 16 hr at 20°C. At the end of the run, the tubes were gently removed from the rotor and the plasmid DNA band was drawn off carefully and extracted as described (Sambrook et al, 1989). Lastly, the DNA pellets were resuspended in TE buffer and stored at 4°C.

## 2.7 Construction of DNA plasmids

The plasmids that were used to produce riboprobes for *in situ* hybridization, were generated according to the common recombinant DNA techniques of Sambrook et al., (1989). Restriction fragments were purified with phenol chloroform (1:1) and ethanol precipitation before being resuspended in TE buffer. PCR products were electrophoresed on 1.5% agarose gels and visualized by ethidium bromide. Subsequently, they were purified with the Geneclean kit (Invitrogen) and resuspended in TE buffer. All PCR products and restriction fragments were subcloned into the vector of choice using T4 DNA ligase & 5X buffer (Gibco/BRL) at 14°C overnight. The ligation reactions were

transformed into the DH5α strain of *E. coli*. Clones were verified by digesting miniprep DNA with specific restriction enzymes and also through sequence analysis.

**2.8 Sequencing**

CsCl purified plasmid DNA used for riboprobe synthesis was sequenced using an ABI 373A automated sequencer with fluorescently dye-labeled dideoxynucleotides and Taq polymerase under manufacturer's directions (Perkin-Elmer Applied Biosystems).

**2.9 Synthesis of primers**

Primers used for PCR were produced on an automated DNA synthesizer (PCR-Mate, model 391, Perkin-Elmer Applied Biosystems) according to manufacturer's directions using the phosphoramidite method. Once primers were synthesized and cleaved with concentrated ammonium hydroxide, they were removed from the column support and deprotected at 55°C overnight with concentrated ammonium hydroxide. The following day, primers were dried, resuspended in $ddH_2O$ and quantitated using a spectrophotometer (Beckman).

## 3. Results

### 3.1 PCR analysis of embryonic *miap3* cDNA

To investigate the role of XIAP during murine development, expression of *miap3* (the murine homolog) was assessed by PCR analysis of prepared cDNA from E7 and E11 total mouse embryos, using *miap3* primers from exon 1 and exon 4. As shown in Figure 4, a 359 bp *miap3* PCR product was amplified from E7 and E11 cDNA (lanes 7 and 8, respectively). In lane 6, *miap3* full length cDNA template was used as a positive control with identical primers used to amplify E7 and E11 cDNA. To control for relative mRNA levels reflected in the cDNA samples and to verify purity of cDNA, β-actin primers were used to amplify mouse genomic DNA, *miap3* full length cDNA and E7 and E11 cDNA. (Figure 4, lanes 1 to 4).

### 3.2 Whole-mount *in situ* detection of *miap3* RNA with a *miap3* specific probe

To explore a possible role for *miap3* in developmental processes, spatial and temporal patterns of *miap3* expression in mouse embryos of different gestational ages was investigated. Visualization of *miap3* RNA distribution by whole-mount *in situ* hybridization in mouse embryos was apparent in embryos at E9.5 to E12. Whole-mount *in situ* hybridization was not used on older embryos due to their size and stage of organogenesis, which would prevent access of the probe to the target RNA.

Since *miap3* 485 bp and 339 bp antisense riboprobes produced identical expression patterns in mouse embryos of E9.5 to E12 and E9.5 to E16.5 with whole-mount and radioactive *in situ* hybridization, respectively, only results obtained with the *miap3* 339 bp riboprobe have been shown (Figure 5). In addition, the 339 bp riboprobe, in the region between BIR3 and the RING zinc finger motif, has a low level of sequence

**Figure 4: PCR analysis of *miap3* expression during days 7 and 11 of mouse embryogenesis**

*Miap3* was amplified at day 7 and 11 of mouse development, observed in lanes 7 and 8. Mouse genomic DNA (500 ng) (lanes 1 and 5), adult mouse *miap3* cDNA (lanes 2 and 6) mouse day 7 (lanes 3 and 7) and 11 (lanes 4 and 8) embryo cDNA (0.3 ng) were subjected to 35 cycles of PCR using β-actin primers (lanes 1-4) and *miap3* exon 1 and 4 specific primers (lanes 5-8). Lanes 9-11were water controls using *miap3* exon-specific primers, human β-actin primers and DMK intron 1 primers respectively. PCR products were analyzed by ethidium bromide agarose gel electrophoresis.
M is designated for 1 Kb molecular weight marker (Gibco/BRL).

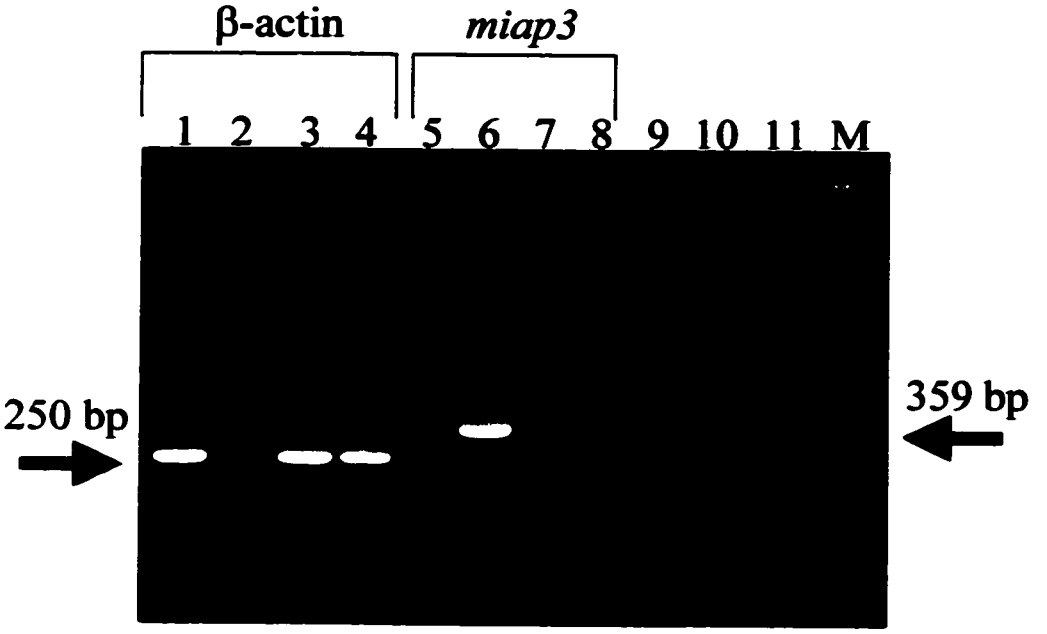
β-actin
miap3
1 2 3 4 5 6 7 8 9 10 11 M
250 bp
359 bp

**Figure 5: Whole-mount *in situ* hybridization using DIG-labeled *miap3* riboprobes on mouse embryos from E9.5, 11 and E11.25**

A) At day 9.5, *miap3* expression was observed in the neuroepithelium surrounding the telencephalic vesicle (tv), mesencephalic vesicle (mv), fourth ventricle (4v), and the optic vesicle (ov). Expression was also detected in the mandibular component of the first branchial arch (m), myocardial wall of the heart (mw), neuroepithelium of the neural tube (nt), and the forelimb bud (flbud) (Mag. X25). B) At day 11-11.25, identical regions had shown *miap3* expression as depicted at day 9.5, with the addition of the maxillary component of first branchial arch (max), second branchial arch ($2^{nd}$brach), wall of the heart/future left ventricle (wh), hindlimb (hl), and the hepatic primordium (hp) (Mag. X15). C) *Myogenin* served as a positive control and exhibited expression in the somites (s) at day 11 (Mag. X15). *Miap3* sense DIG riboprobe was used as a negative control to reveal nonspecific labeling or activity of endogenous alkaline phosphatase.

A antisense sense

E9.5

antisense

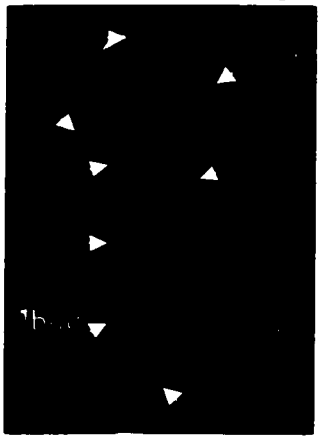

E9.5

B antisense antisense sense

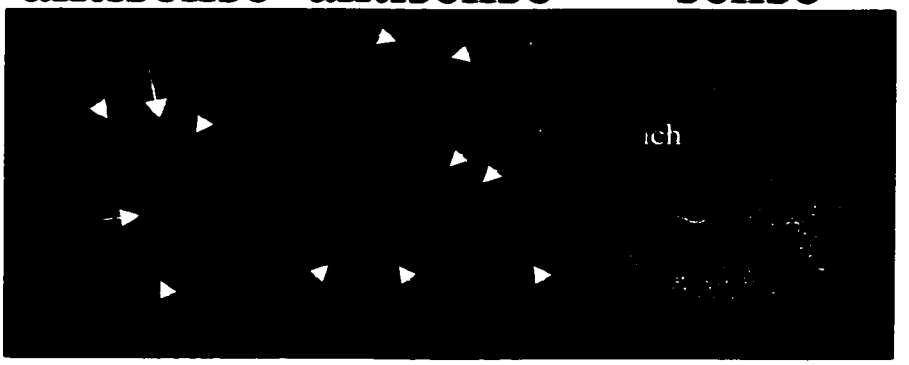

E11 E11.25 E11

C antisense sense

E11

antisense

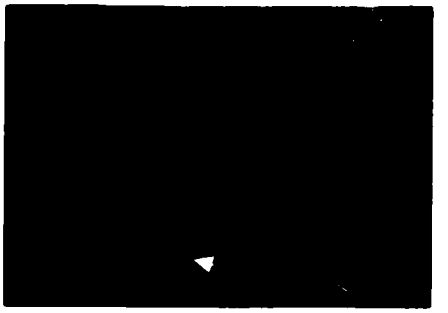

E11

homology with respect to the other human IAPs and therefore was choosen for *in situ* hybridization.

*Miap3* expression within mouse embryos of E9.5 to E12 was verified by whole-mount *in situ* with the DIG-labeled antisense *miap3* 339 bp riboprobe, the location of which is shown in Figure 5 and 6. As a negative control, sense *miap3* 339 bp riboprobe was used. *Miap3* expression was noted at E9.5, the earliest time point examined, in many of the developing CNS structures. For example, expression was observed in the telencephalic (tv) and mesencephalic (mv) vesicles as well as in the fourth ventricle (4v) and optic vesicle (ov) (Figure 5A). In addition, *miap3* transcripts were evident in the mandibular component of the first branchial arch (m), myocardial wall of the heart (mw), neuroepithelium of the neural tube (nt) and forelimb bud (flbud) (Figure 5A).

A similar distribution pattern of *miap3*, observed at day 9.5, was noted at E11 to E11.25, including staining in the second branchial arch (2ndbrach), hepatic primordium (hp), and the hindlimb bud (hl) (Figure 5B). For E9.5 and E11 to E11.25, the sense *miap3* riboprobe failed to hybridize in the pattern observed with the antisense probe(s) (Figure 5A sense and 5B sense). Omission of the riboprobes and the anti-DIG Fab fragments served as additional negative controls that revealed nonspecific labeling (data not shown). Furthermore, *myogenin* was used as a positive control and expression was seen within the myotomes of the somites (s) of E11 embryos (Figure 5C), reproducing findings of Sassoon et al., (1989).

In the developing head of E11.5 to E12 embryos, expression of *miap3* becomes more noticeable. The features that are more prominent include the maxillary component of the first branchial arch (max), metencephalon (met), wall of the midbrain (wm), optic

stalk (os), nasal process (np), and the neopallial cortex (nc) (Figure 6A). Once again, the forelimb bud (flbud), hindlimb bud (hl) and wall of the heart (wh) had revealed *miap3* expression as noted for E11 to E11.25. In addition to the brain structures mentioned for E11.5 to E12, the inner structures of the head region had revealed staining in the myelencephalon (my) or future medulla oblongata, and Rathke's pouch (rp) or future anterior pituitary (Figure 6B). The expression of *miap3* had also appeared in the mantle layer of the spinal cord (mlsc), mandibular component of the first branchial arch (m), lung bud (Lbud), centrum of nerves (cn), hepatic primordium (hp), and in the developing midgut/hingut region (mhg) (Figure 6B). No specific staining was noticed in the sense control that accompanied the E11.5 to E12 antisense hemi-sectioned embryos (Figure 6B). Again, the *myogenin* was used as a control with embryos of E11.5 to E12, showing its characteristic localization pattern.

**3.3 Detection of *miap3* RNA by radioactive *in situ* hybridization**

Radioactive *in situ* hybridization was chosen because of the high level of sensitivity it provides in comparison to whole-mount *in situ* hybridization. Mouse embryo sections that were incubated with radioactively labeled *miap3* 339 bp antisense riboprobe showed a strong expression pattern, the location of *miap3* transcript where whole-mount sections had displayed an overall weak staining pattern. Therefore, radioactive *in situ* was used to further view which developing tissues contained *miap3* transcript.

The overall location of *miap3* in mouse embryos from E9.5 to E16 was generally ubiquitous. At E9.5, *miap3* was detected in the neuroepithelial lining of the forebrain (nf), midbrain (nm), hindbrain (hf), and otic vesicle (ov) (Figure 7A). Other sites of distribution were in the mandibular component of the first branchial arch (m), myocardial

**Figure 6: Whole-mount *in situ* hybridization using a Dig-labeled *miap3* riboprobe on mouse embryos from E11.5 to E12**

A) *Miap3* expression was observed in the: maxillary component of the first branchial arch (max), metencephalon/future pons/cerebellar junction (met), wall of the midbrain/mesencephalon (wm), optic stalk (os), nasal process (np), neopallial cortex/future cerebral cortex (nc), wall of the heart (wh), forelimb bud (flbud), and hindlimb bud (hl) (Mag. X11). The 339 bp *miap3* antisense riboprobe was used to detect expression and the 339 bp *miap3* sense riboprobe served as a negative control. B) Mouse embryos of E11.5-12 were hemi-sectioned longitudinally before the hybridization treatments of day 1 had begun. There was additional *miap3* expression observed internally: Rathke's pouch/future anterior pituitary (rp), mandibular component of first branchial arch (m), myelencephalon/future medulla oblongata (my), centrum of axis/nerves (cn), lung bud (Lbud), hepatic primordium (hp), mantle layer of the spinal cord (mlsc), and midgut/hindgut (mhg) (Mag. X11). C) *Myogenin* antisense riboprobe, in comparison to the *myogenin* sense riboprobe revealed expression in the intercostal muscles (inm), muscles of the forelimb & hindlimbs (mus), and in somites (s) (Mag. X11) of E12 mouse embryos.

A antisense sense antisense

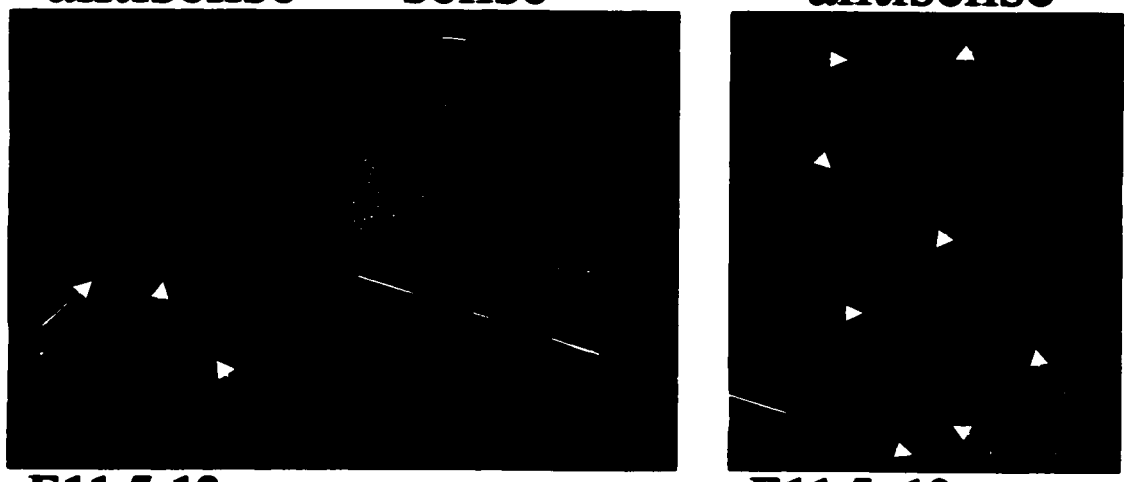

E11.5-12 E11.5 -12

B antisense antisense sense

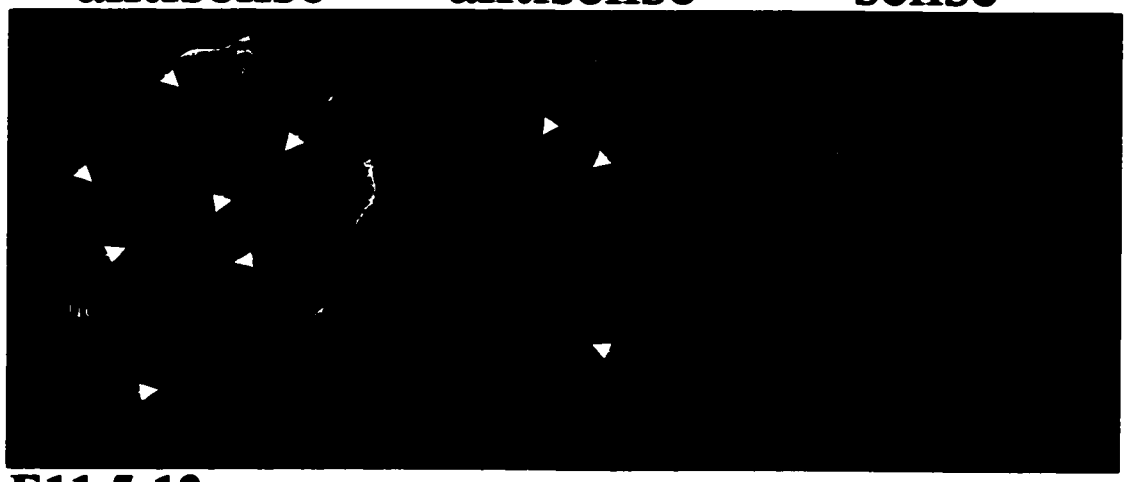

E11.5-12

C antisense sense antisense

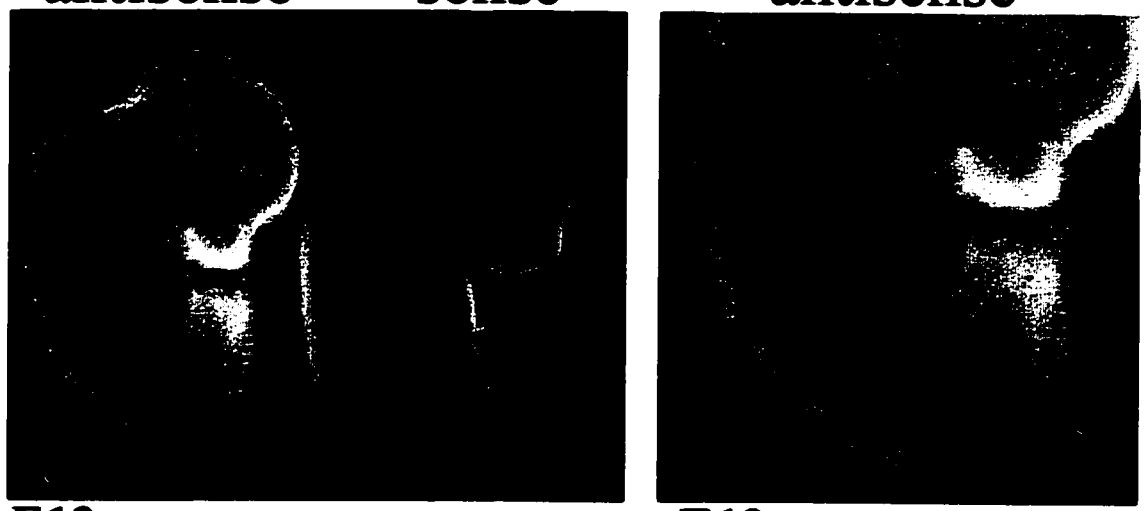

E12 E12

**Figure 7: *In situ* localization of *miap3* during murine embryogenesis**

Sagittal (a-f) sections (6 μm) of embryos at the indicated stages were hybridized with a $^{33}$P-labeled *miap3* coding region (339 bp) antisense and sense riboprobes (left to right). **A)** At E9.5 *miap3* expression was observed in the neuroepithelium that surrounds the fourth ventricle (4thV), the telencephalic vesicle (tv), the hindbrain (nh) and the forebrain (nf) respectively. Expression was detected in the neuroepithelium of the midbrain region (nm), and the otic vesicle (ov), mandibular component of the first branchial arch (m), myocardial wall of ventricular chamber of the heart (mw), midgut/hindgut junction (mhg), and the neuroepithelium of the neural tube (nt) (Mag. X30). **B)** In addition to the expression observed at E9.5, at E11 *miap3* was noticed in the optic stalk (os), body wall (thoracic) overlying the pericardial cavity (tbw), future left ventricle (flv), nasal process (np), lung bud (Lbud), developing stomach and intestines (dsi), dorsal root ganglia (drg), hepatic primordium (hp), and neuroepithelium (ne) (Mag. X30). **C)** At E13, expression was detected in the neopallial cortex/future cerebral cortex (nc), medulla oblongata (mo), choroid plexus differentiating from roof of fourth ventricle (cp), roof of midbrain (mid), pons (p), olfactory epithelium (oe), Rathke's pouch (rp), lower jaw (lj), intrinsic muscles of the tongue (t), left lung (ll), heart (h), left lobe of liver (L), cartilage primordium of body vertebra (cpb), developing stomach (ds), mantle layer of spinal cord (mlsc), and the notochord (nch) (Mag. X30). **D)** In addition to the expression observed at E13, at E14 *miap3* was observed in the priomordia of follicles of vibrissae (fov), skin/ectoderm (e), wall of left atrium (wla) dorsal root ganglia (drg), diaphragm (d), and the digits of the hind limb and forelimb (dhl), (dfl) (Mag. X 30). **E)** At E16, the additional tissues displayed *miap3* expression: cerebellar primordium (cp), lower lip (lol), wall of left ventricle and atrium (lv), (wla), thymus (thy), left lung (LL), intestines (int), and the left kidney (lk) (Mag. X30). **F)** This panel served as a positive control using the *myogenin* antisense and sense riboprobes. Expression of *myogenin* was noticed quite prominently in the intercostal muscles (inm), intrinsic muscles of the tongue (t), diaphragm (d), and the primordia of follicles of vibrissae (fov) (Mag X30).

A antisense sense

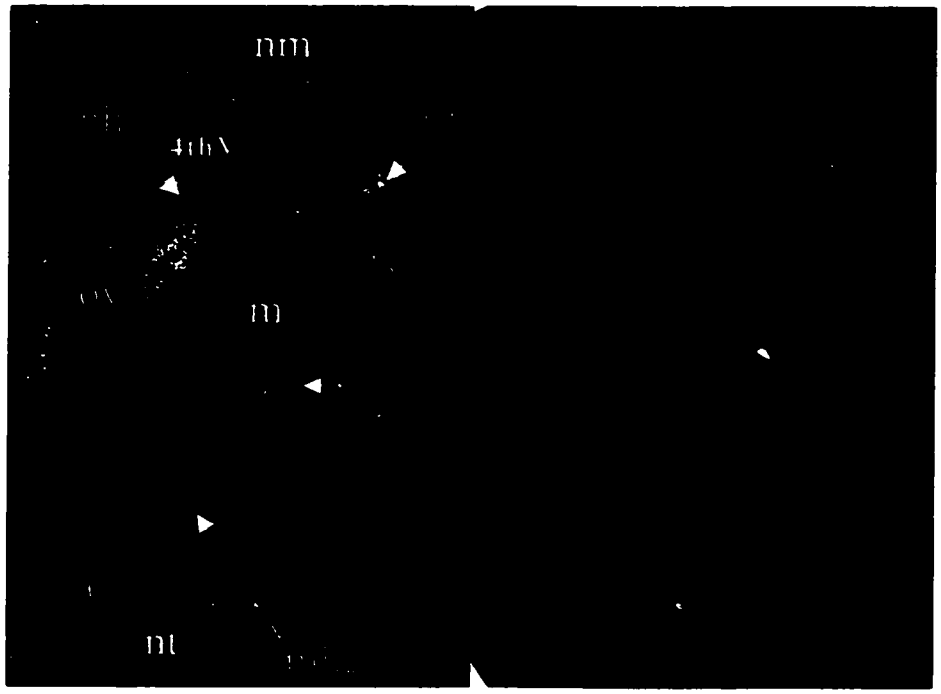


B antisense sense

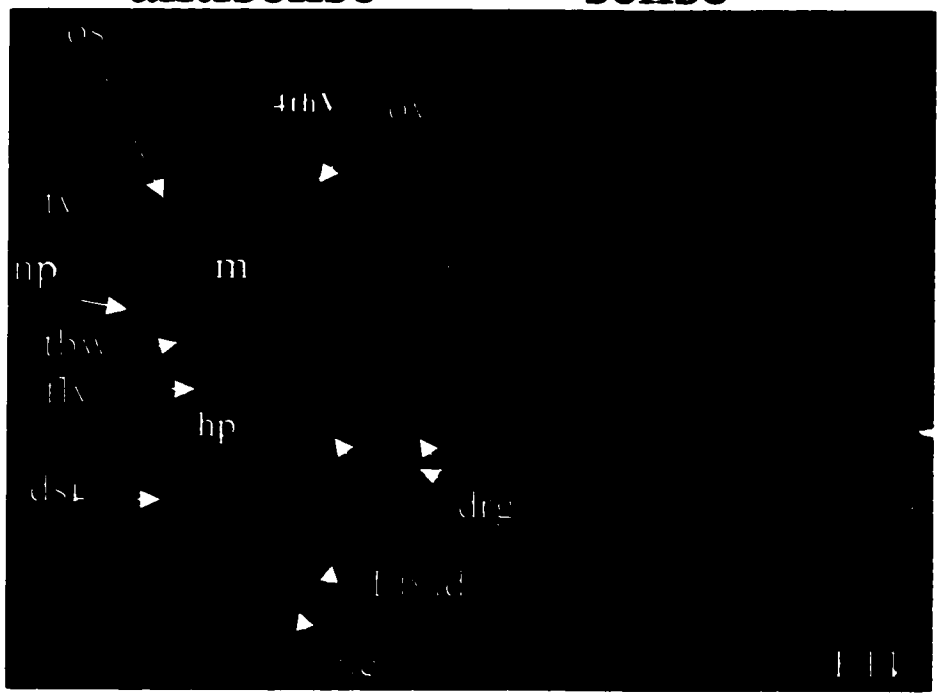

wall of the heart (mw), neural epithelium of the neural tube (nt), and in the developing midgut and hindgut junction (mhg) (Figure 7A). To confirm *miap3* specificity, sense labeled sections were shown to be negative for *miap3* transcript that was easily observed on antisense labeled sections (Figure 7A).

At E11, the regions to which *miap3* localized were quite similar to those of E9.5. In addition to those sites, *miap3* was discovered in the latest developing tissues including the nasal process (np), the body wall overlying the pericardial cavity (tbw), the future left ventricle (flv), although to a varying degree compared to the other tissues examined. In addition, the hepatic primordium (hp), lung bud (Lbud), developing stomach and intestines (dsi), and the dorsal root ganglia (drg) towards the posterior end of the embryo contained *miap3* RNA (Figure 7B). *Miap3* transcripts were not detectable in the sense labeled sections for E11 (Figure 7B, right panel).

During embryonic day 13 there were certain structures in the mouse brain, aside from the previous ones mentioned at E11, that showed the presence of *miap3* transcript. Analysis of the E13 sagittal section identified *miap3* in the developing pons (p) region, Rathke's pouch (rp) or future anterior pituitary, the neopallial cortex (nc), later known as the cerebral cortex, and differentiating from the roof of the fourth ventricle, the choroid plexus (cp) (Figure 7C). Other tissues that continued to display *miap3* transcript were the olfactory epithelium (oe), situated in the nasal process (np), the developing tongue (t) and lower jaw (lj). Furthermore, the heart (h) and body wall overlying the pericardial cavity (tbw), as well as the liver (L), left lung (ll), developing stomach (ds) and mantle layer of the spinal cord (mlsc) were tissues that continued to display *miap3* (Figure 7C). In this

C antisense sense

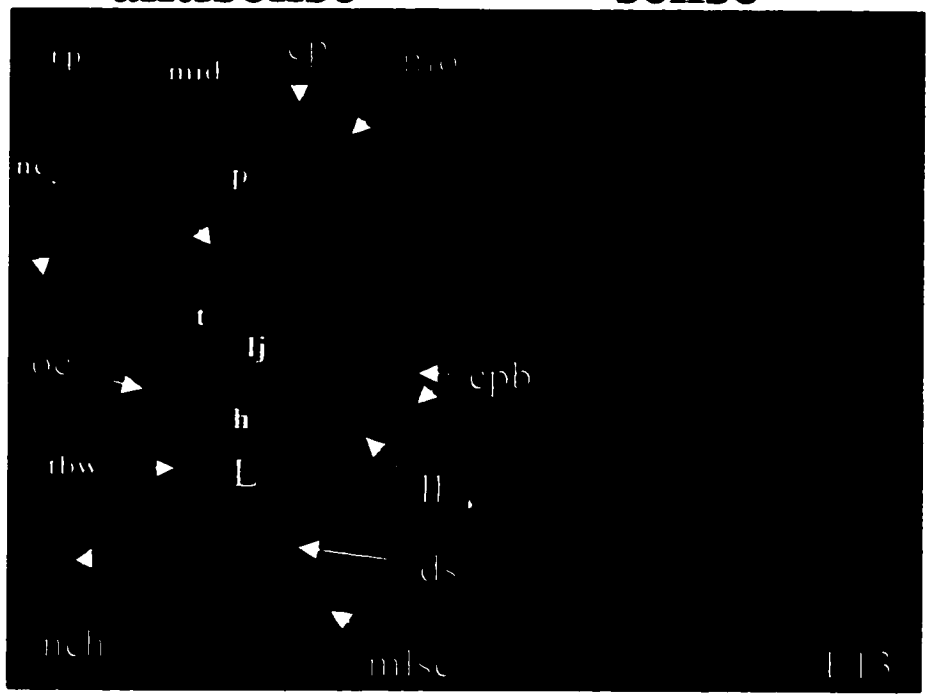


D antisense sense

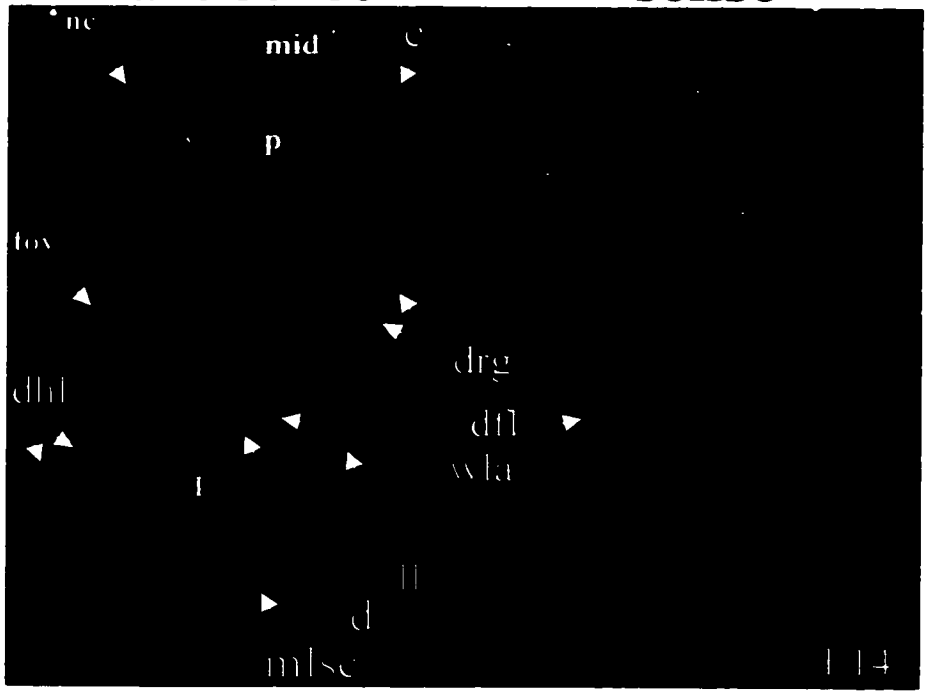

particular section the cartilage primordia of the vertebra (cpb) and the notochord (nch) were apparent and also exhibited *miap3* expression.

As shown in Figure 7D, *miap3* transcripts were still observed in the developing brain structures mentioned for E13. The follicles of vibrissae (fov) in the snout, the diaphragm (d) and the digits of the forelimb (dfl) and hindlimb (dhl) were newly developed tissues that were positive for *miap3* mRNA (Figure 7D). In addition, the left lung (ll), wall of the left atrium (wla), and upper spinal dorsal root ganglia (drg) in Figure 7D showed *miap3* expression. Antisense sections (left panels, Figure 7C and 7D) were compared to their serial section *miap3* sense control counterparts (right panels) for nonspecific labeling, which was not observed.

Mouse embryos at E16.5 were labeled with the same *miap3* antisense riboprobe that was used for earlier days. The pattern of *miap3* expression at this stage was not noticeably different in comparison to the preceding times. The only exception would be the slightly higher levels of *miap3* transcript observed in the upper spinal dorsal root ganglia (drg) (Figure 7E). Apart from the tissues mentioned in E13, the cerebellar primordium (cp), thymus (thy), left kidney (lk), and developing intestines (int) were identified with *miap3* transcript (Figure 7E). The distribution of *miap3* transcript at E16.5 was very distinct to the pattern of *myogenin* expression as shown in Figure 7F. The presence of *myogenin* transcript was clearly seen in the developing muscles of the tongue (t), diaphragm (d), neck, facial muscles, as well as intercostal muscles (inm) (Figure 7F). An overall summary of *miap3* expression in the developing mouse embryo is shown in Table I.

E antisense sense

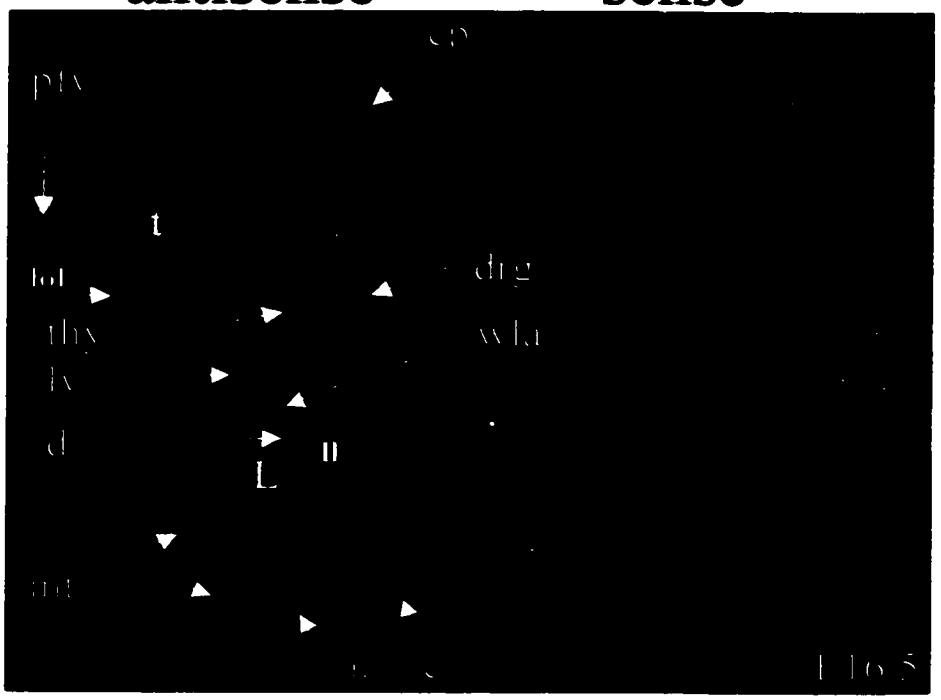

F antisense sense

**Table I. A summary of *miap3* expression in the developing mouse embryo as determined by *in situ* hybridization analysis and immunofluorescence**

Expression of *miap3* was detected with *in situ* hybridization using the 339 bp antisense riboprobe and also with immunofluorescence employing the RIAP3 antibody. The results do not show any significant differences in the levels of *miap3* during the particular embryonic times, although there was a slight decrease in *miap3* expression after day13.5 in various developing tissues. Similar results were obtained in three independent experiments. This data is from one of those experiments.
+, weak staining; ++, moderate staining; +++, strong staining; NA, not applicable; NS, not shown

Table I. Localization of *miap3* transcript and protein in murine embryos from embryonic 9.5- to 16.5-day(d)

| | Transcript | | | | | Protein | | | | |
|---|---|---|---|---|---|---|---|---|---|---|
| | 9.5d | 11d | 12d | 13.5d | 16.5d | 9.5d | 11d | 12d | 13.5d | 16.5d |
| Central nervous system | | | | | | | | | | |
| Neuroepithelium | ++ | +++ | +++ | ++ | + | +++ | +++ | +++ | ++ | + |
| Neopallial cortex/ Cerebral cortex | NA | ++ | ++ | ++ | + | NA | +++ | +++ | +++ | NA |
| Choroid plexus | NA | NA | NA | ++ | NS | NA | NA | NA | +++ | NS |
| Medulla oblongata | NA | ++ | +++ | ++ | NS | NA | +++ | ++ | +++ | NS |
| Spinal cord | ++ | ++ | ++ | +++ | ++ | ++ | +++ | +++ | +++ | + |
| Peripheral nervous system | | | | | | | | | | |
| Dorsal root ganglia | NA | ++ | ++ | +++ | NS | NA | ++ | ++ | +++ | NS |
| Cervical drg | NA | ++ | ++ | +++ | ++ | NA | ++ | NS | NS | ++ |
| Eye and Nose | | | | | | | | | | |
| Retina | NS | NS | NS | ++ | NS | NS | NS | NS | ++ | NS |
| Lens | NS | NS | NS | ++ | NS | NS | NS | NS | +++ | NS |
| Pigmented epithelium | NS | NS | NS | +++ | NS | NS | NS | NS | +++ | NS |
| Olfactory epithelium | NS | NS | NS | +++ | + | NS | NS | NS | +++ | + |
| Musculoskeletal system | | | | | | | | | | |
| Skeletal muscle | ++ | ++ | ++ | ++ | + | ++ | ++ | ++ | ++ | + |
| Tongue | NA | NA | ++ | ++ | + | NA | NA | ++ | ++ | + |
| Diaphragm | NA | NA | + | ++ | + | NA | NA | + | ++ | + |
| Cartilage of vertebra | NA | ++ | ++ | ++ | + | NA | ++ | ++ | ++ | + |
| Lower jaw | NA | NA | NA | ++ | ++ | NA | NA | NA | ++ | + |
| Cardiovascular system | | | | | | | | | | |
| Heart muscle/ Ventricles | + | ++ | ++ | ++ | + | + | ++ | ++ | ++ | + |
| Atriums | + | ++ | ++ | ++ | + | + | ++ | ++ | ++ | + |
| Gastrointestinal system | | | | | | | | | | |
| Stomach | + | ++ | NS | ++ | NS | + | ++ | NS | ++ | NS |
| Intestines | NS | ++ | NS | NS | ++ | NS | ++ | NS | NS | ++ |
| Liver | NA | ++ | ++ | ++ | + | NA | ++ | ++ | ++ | + |
| Hematolymphoid system | | | | | | | | | | |
| Thymus | NA | NA | NA | NA | ++ | NA | NA | NA | NA | + |
| Mesenchyme | | | | | | | | | | |
| Kidney | NA | NA | NS | NS | + | NA | NA | NS | NS | + |
| Lung | NA | ++ | NS | ++ | ++ | NA | ++ | NS | ++ | ++ |
| Skin | | | | | | | | | | |
| Epidermis | ++ | ++ | ++ | ++ | + | ++ | ++ | ++ | ++ | + |
| Hair follicles | NA | NA | NA | NS | + | NA | NA | NS | ++ | + |

### 3.4 Western blot analysis of adult mouse tissues and embryos from E9 to E13

Total cytosolic protein was isolated from various tissues of CD-1 mice and analyzed by Western blot for the expression of MIAP3 with an anti-RIAP3 (affinity purified) polyclonal antibody. As shown in figure 8A and B, a 55 kDa band was detected in all of the adult mouse tissues. However, the expression of MIAP3 was sufficiently lower in adult intestines and slightly less in the adult heart. Tissue extracts were probed with an anti-α-actin antibody to control for protein loading (Figure 8A and B). A few of the adult tissues exhibited a species at ~85-90 kDa, suggesting that it may be a cross-reactive band.

To determine whether the embryos expressed MIAP3 protein, total embryo extracts from E9, 10, 11 and 13 were analyzed with the anti-RIAP3 antibody. A distinct species of 55 kDa was identified for all four embryonic days, and was also normalized. The same blot was probed with anti-α-actin antibody to control for protein loading (Figure 8C).

### 3.5 Detection of MIAP3 protein expression in mouse embryo sections

Having established that *miap3* transcript is ubiquitously present during different gestational ages in mouse development, we questioned the possibility of whether MIAP3 protein was co-localizing with *miap3* transcript. Anti-RIAP3 was used to localize MIAP3 protein by immunohistochemistry and immunofluorescence on mouse embryo sections from E9, 11, 12, 13.5, and E16.5.

At E9.5, MIAP3 immunoreactivity was detected in many of the same areas that the *miap3* transcript was found to localize (Figure 9A and B). Prominent staining was observed in the neuroepithelium of the neural tube (ne), as well as in the mandibular

**Figure 8: Expression of MIAP3 protein in adult mouse tissues**

Total cytosolic protein extracts (25μg) isolated from various normal mouse tissues were analyzed for MIAP3 expression by western blot analysis. **A)** The tissue extracts were: lane 1, testes; lane 2, diaphragm; lane 3, stomach; lane 4, intestine; lane 5, lung; lane 6, spinal cord; lane 7, muscle. **B)** The tissue extracts are seen in: lane 1, liver; lane 2, spleen; lane 3, thymus; lane 4, heart; lane 5, brain; lane 6, kidney. Both blots were probed with anti-RIAP3 and the same blots were stripped and incubated with an anti-α-actin antibody (Sigma) for normalization. Detection of MIAP3 and α-actin protein was performed using an enhanced chemiluminescent system with a horse radish peroxidase-coupled goat anti-rabbit antibody and a horse radish peroxidase-coupled goat anti-mouse antibody, respectively. **C)** Total embryonic protein extracts (25μg) isolated from E9 to E13 were analyzed for MIAP3 expression by western blot analysis. Lane 1, E9; lane 2, E10; lane 3, E11; lane 4 E13. The membrane was probed with anti-RIAP3 and was stripped and re-probed with anti-α-actin antibody for normalization. The same detection system was incorporated as stated in B).

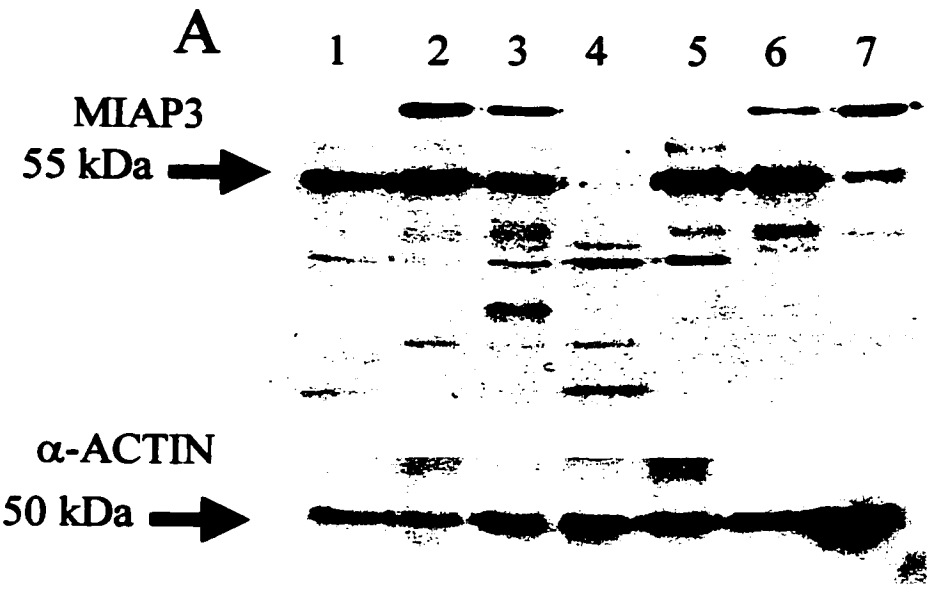
A
1
2
3
4
5
6
7
MIAP3
55 kDa
α-ACTIN
50 kDa

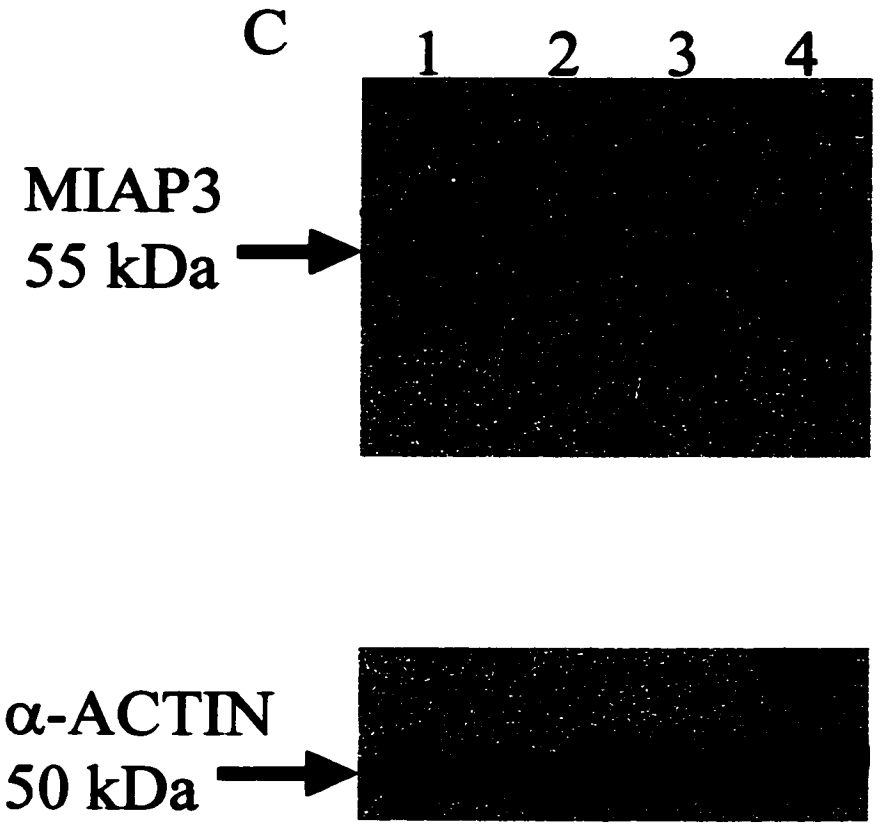
C
1
2
3
4
MIAP3
55 kDa
α-ACTIN
50 kDa

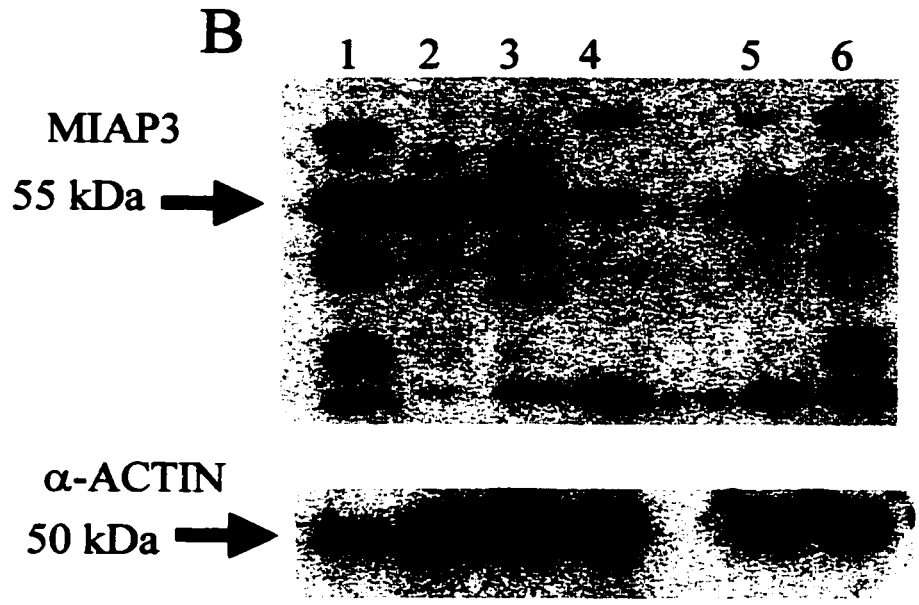
B
1 2 3 4 5 6
MIAP3
55 kDa
α-ACTIN
50 kDa

**Figure 9: *In situ* localization and immunohistochemical analysis of *miap3* on mouse embryo sections from E9.5 and E11-11.5**

Panels A and C are sagittal sections probed with $^{33}$P-labeled antisense *miap3* 339 bp riboprobe. Panels B and D were labeled with affinity-purified anti-RIAP3 antibody followed by 3'-3'-diaminobenzidine staining. **B)** At E9.5 MIAP3 protein was observed in the following regions: neuroepithelium (ne) of the midbrain (nm), forebrain (nf), and neural tube, and (nt), mandibular component of the first branchial arch (m), myocardial wall of the ventricular chamber of the heart (mw), and wall of the right atrium (wra) (Mag. X30). **D)** In addition, at E11.5 MIAP3 protein appeared in the neuroepithelium of the hindbrain (nh), nasal process (np), future left ventricle (flv), wall of the left atrium (wla), body wall (thoracic) overlying the pericardial cavity (tbw), hepatic primordium (hp), developing stomach (ds), centrum of axis/nerve (cn), dorsal root ganglion (drg), somites (s) (Mag. X30).

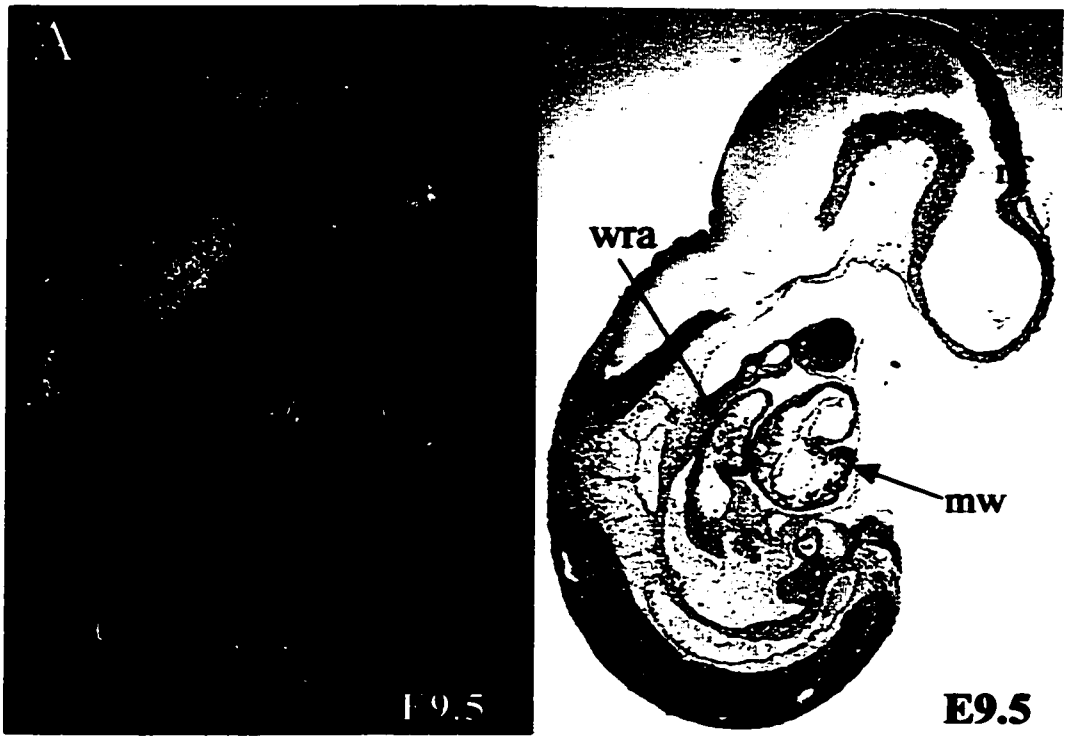
A
E9.5
wra
mw
C
E11.5
D
flv
wla
ds
hp
cn
drg
s
E11.5

component of the first branchial arch (m), the wall of the right atrium (wra) and the myocardial wall of the developing ventricle (mw) (Figure 9B). Expression of MIAP3 protein was slightly lower in intensity in the neuroepithelium of the brain in comparison to the tissues mentioned previously at E9.5. Figure 9D demonstrates the presence of MIAP3 protein in several of the developing tissues of E11.5. MIAP3 protein was observed in the nasal process (np), neuroepithelium of the hindbrain (nh), thoracic wall (tbw), developing stomach (dsi) and the centrum of axis (cn). In addition, the mandibular component of the first branchial arch (m), future left ventricle (flv), hepatic primordium (hp), posterior dorsal root ganglia (drg), and neuroepithelium exhibited a slightly higher level of MIAP3 expression (Figure 9D).

Further analysis of E11 mouse sections, (however, this time by immunofluorescence) revealed MIAP3 protein in identical structures that contained *miap3* transcript (Figure 10A to E). Mouse brain sections showed brightly stained neuroepithelium surrounding the telencephalic vesicle (tv), fourth ventricle (4thV) and future medulla oblongata (my) (Figure 10A to C). Immunohistochemical and immunofluorescence staining of the mandibular component (m), future ventricle (frv), dorsal root ganglia (drg), and neuroepithelium (ne) appeared to be analogous in terms of localization of MIAP3 protein. Other tissues showing MIAP3 immunoreactivity were the lung bud (Lbud), centrum of axis (cn), and the thoracic wall (tbw) (Figure 10D and E). To confirm the specificity of our antibody to MIAP3, preimmune serum was added in place of the anti-RIAP3 antibody on serial sections. As verified in Figure 10C (far right), immunofluorescence was reduced considerably. In addition, anti-RIAP3 was preabsorbed with RIAP-3-GST protein to confirm that the observed staining was due to

**Figure 10: *In situ* localization and immunofluorescence analysis of *miap3* on mouse sections of E11**

Mouse embryo sagittal sections, shown left to right, were labeled with $^{33}$P-labeled *miap3* 339 bp antisense and sense riboprobes. Immunofluorescence (I.F) was observed in the panel farthest to the right. Sections were labeled with anti-RIAP3 antibody followed by a CY3-labeled sheep anti-rabbit secondary antibody. *Miap3* RNA and protein expression patterns were identical in the following regions. **A)** neopallial cortex/future cerebral cortex (nc): ventricular zone (vz), cortical plate (cpl), and intermediate zone (iz) (Mag. X10). **B)** Fourth ventricle (4thV), cerebellar primordium (cp), and myelencephalon/future medulla oblongata (my) (Mag. X10). **C)** Wall of midbrain (wm), and mesencephalic vesicle (Mag. X10). **D)** Mandibular component of the first branchial arch (m), body wall (thoracic) overlying pericardial cavity (tbw), future right ventricle (frv), and hepatic primordium (hp) (Mag. X10). **E)** Neuroepithelium (ne), centrum of axis/nerves (cn), dorsal root ganglion (drg), and lung bud (Lbud) (Mag. X10).

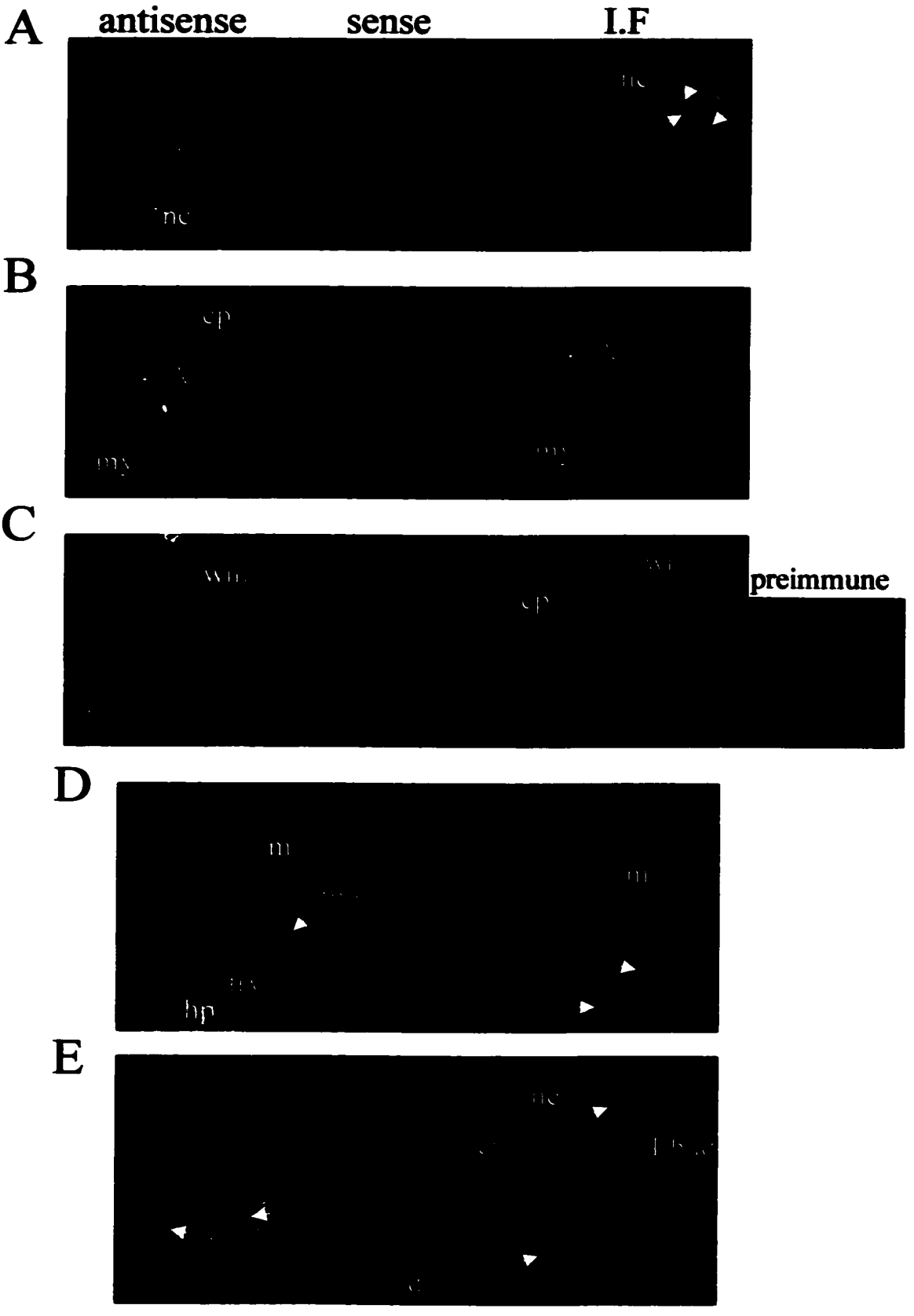
A
antisense
sense
I.F
nc
nc
B
cp
my
my
C
preimmune
cp
D
m
m
hp
E
nc

immunoreactivity of anti-RIAP3 antibody (data not shown).

MIAP3 immunoreactivity in E12 sections coincided with the uniform expression observed at E11 [Figure 11A-E (I.F)]. Although, a slightly higher level of immunofluorescence was observed in the neopallial cortex (nc) or future cerebral cortex in relation to the other tissues examined [Figure 11A (I.F)]. Investigation at higher magnification revealed that MIAP3 protein was localized within the cytoplasm, clearly visible in the mandible (Figure 11C).

At E13.5, staining remained prominent in the neopallial cortex (nc) and was apparent in the choroid plexus (cp) that had descended into the lateral ventricle (lv) (Figure 12A). Expression of MIAP3 was also observed in the choroid plexus (cp), which had differentiated from the roof of the fourth ventricle (4thV) (Figure 12B). An increased level of MIAP3 expression was observed in the olfactory epithelium (oe) in contrast to the nasal region (Figure 12C). In addition, a bright staining pattern was visualized in the developing eye, more specifically, in the lens fibres (lf), and in the pigment (plr) and neural layers of the retina (nlr) (Figure 12D). MIAP3 continued to be expressed in the muscles of the tongue (mt), left ventricle (lv), and liver (L), where protein was located within the cytoplasm viewed under higher magnification (Figure 12E and F). MIAP3 was still seen in the lung (LL), although mainly in the tissue surrounding the branches of the segmental bronchi, as well as in the dorsal root ganglia (drg) and mucous layer of the stomach (mls) (Figure 12G to I).

Analysis of MIAP3 expression in mouse sections at E16.5 suggested that lower levels of protein were expressed in certain tissues in relation to the same tissue types examined at E13.5. The developing upper (ul) and lower lips (lol) from the mandibular

**Figure 11: *In situ* localization and immunofluorescence analysis of *miap3* on mouse sections of E12**

Mouse embryo sagittal sections, shown left to right, were labeled with $^{33}$P-labeled *miap3* 339 bp antisense and sense riboprobes. Immunofluorescence (I.F) was observed in the panel farthest to the right. Sections were labeled with anti-RIAP3 antibody followed by a fluorescein-labeled goat anti-rabbit secondary antibody. *Miap3* RNA and protein expression patterns were identical in the following regions. **A)** Neopallial cortex/future cerebellar cortex (nc), and tissue surrounding the telencephalic vesicle/lateral ventricle (tv) (Mag. X10). **B)** Tissue surrounding the fourth ventricle (4thV), myelencephalon/future medulla oblongata (my) and metencephalon/cerebellar primordium (met) (Mag. X10). **C)** Mandibular component of the first branchial arch (m) (Mag. X10). **D)** Lateral ventricle (lv) and liver (L), staining of heart and liver with preimmune serum shown next to the I.F section (Mag. X10). **E)** Lung bud (Lbud), dorsal root ganglion (drg), and neuroepithelium (ne) (Mag. X10).


A
antisense
sense
LF
B
C
D
preimmune
E

**Figure 12: *In situ* localization and immunofluorescence analysis of *miap3* on mouse sections of E13.5**

Mouse embryo sagittal sections, shown left to right, were labeled with $^{33}$P-labeled *miap3* 339 bp antisense and sense riboprobes. Immunofluorescence (I.F) was observed in the panel farthest to the right. Sections were labeled with anti-RIAP3 antibody followed by a CY3-labeled sheep anti-rabbit secondary antibody. *Miap3* RNA and protein expression patterns were identical in the following regions. **A)** Choroid plexus (cp) extending into the lateral ventricle (lv), and neopallial cortex/future cerebellar cortex (nc) (Mag. X10). **B)** Choroid plexus (cp) differentiating from roof of fourth ventricle (4thV) (Mag. X10). **C)** Nasal process (np) and olfactory epithelium (oe) (Mag. X10). **D)** Pigment layer of retina (plr), neural layer of retina (nlr), and lens fibres (lf) (Mag. X10). Preimmune staining of eye served as a negative control against anti-RIAP3 antibody. **E)** Muscle of tongue (mt), and lower lip (lol) (Mag. X10). **F)** Left ventricle (lv) and liver (L). A 100X magnification of the liver revealed cytoplasmic expression of MIAP3. **G)** left lung (LL) (Mag. X10). **H)** Dorsal root ganglion (drg) and mantle layer (ml) (Mag. X10). **I)** Lumen of stomach (ls) and mucous lining of the stomach (mls) (Mag. X10).

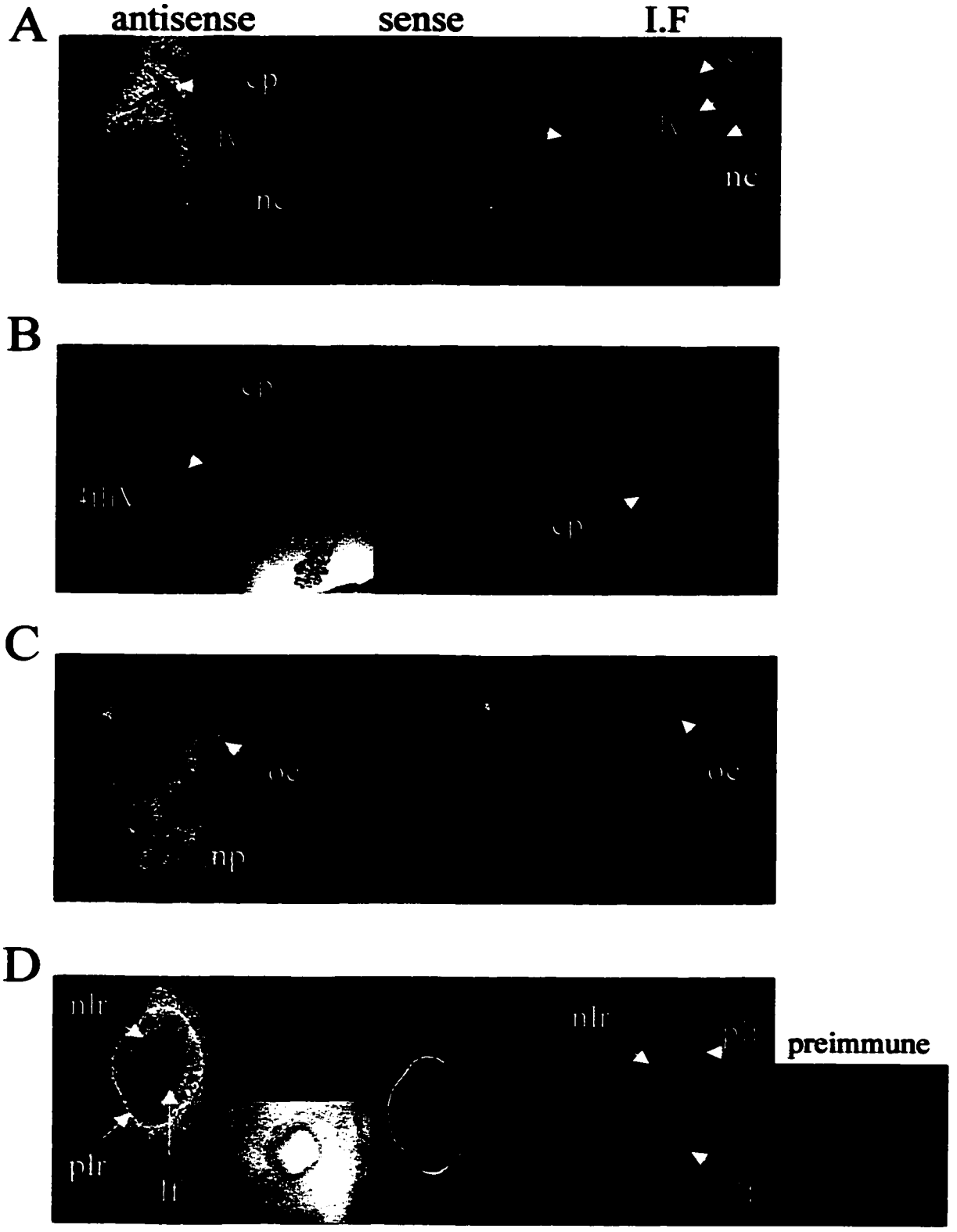
A
antisense
sense
I.F
cp
nc
nc
B
cp
cp
C
nc
nc
np
D
nlr
nlr
plr
preimmune

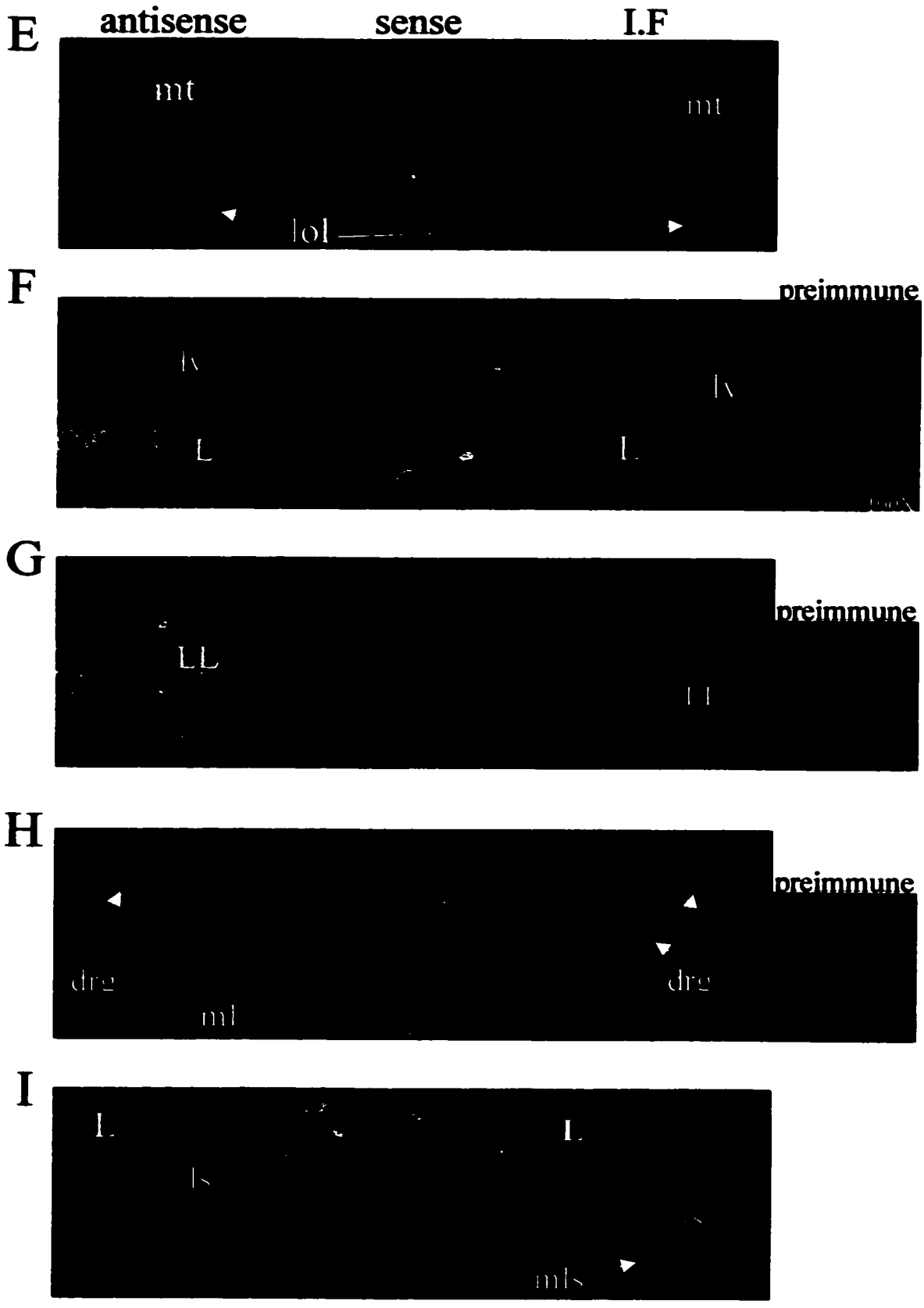
E
antisense
sense
I.F
mt
mt
lol
F
preimmune
lv
lv
L
L
G
preimmune
LL
LL
H
preimmune
drg
drg
ml
I
L
L
ls
mls

**Figure 13: *In situ* localization and immunofluorescence analysis of *miap3* on mouse sections of E16.5**

Mouse embryo sagittal sections, shown left to right, were labeled with $^{33}$P-labeled *miap3* 339 bp antisense and sense riboprobes. Immunofluorescence (I.F) was observed in the panel farthest to the right. Sections were labeled with anti-RIAP3 antibody followed by a CY3-labeled sheep anti-rabbit secondary antibody. *Miap3* RNA and protein expression patterns were identical in the following regions. **A)** Follicles of vibrissae associated with the upper lip (fov) and upper lip (ul) (Mag. X10). **B)** Muscles of the tongue (mt) and lower lip (lol) (Mag. X10). **C)** Lung (lu) (Mag.X10). **D)** Thymus gland (thy) and wall of right atrium (wra) (Mag. X10). **E)** Liver (L) and diaphragm (d) (Mag. X10). **F)** Intercostal muscles (inm) and cartilage primordium of ribs (cpr) (Mag. X10). **G)** Kidney (kid) (Mag. X10). **H)** Intestines: epithelial cells of intestinal villi (int) (Mag. X10). **I)** Cervical dorsal root ganglion (cdrg) (Mag. X10).

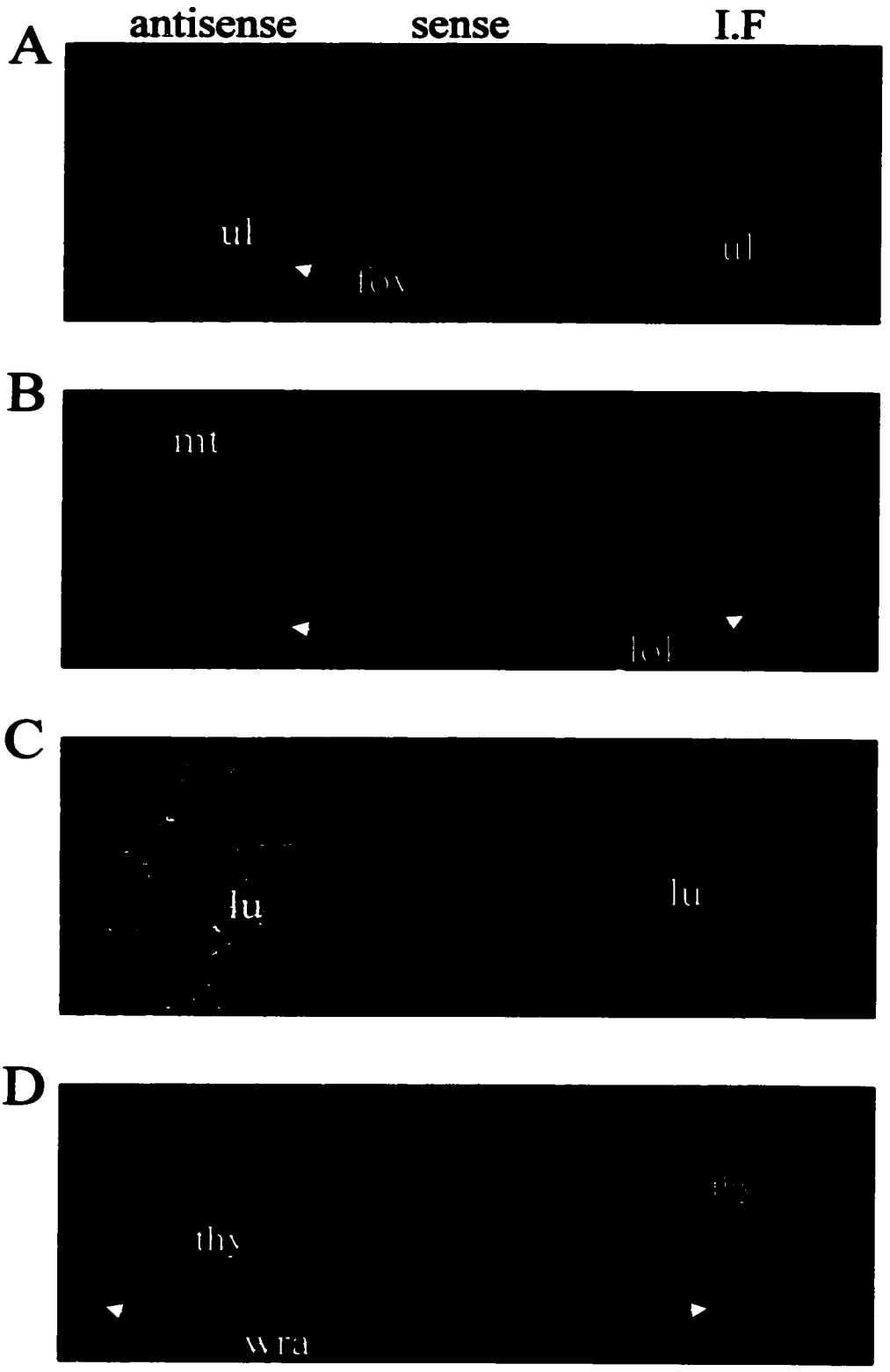
A
antisense
sense
I.F
ul
fox
ul
B
mt
lol
C
lu
lu
D
thy
wra

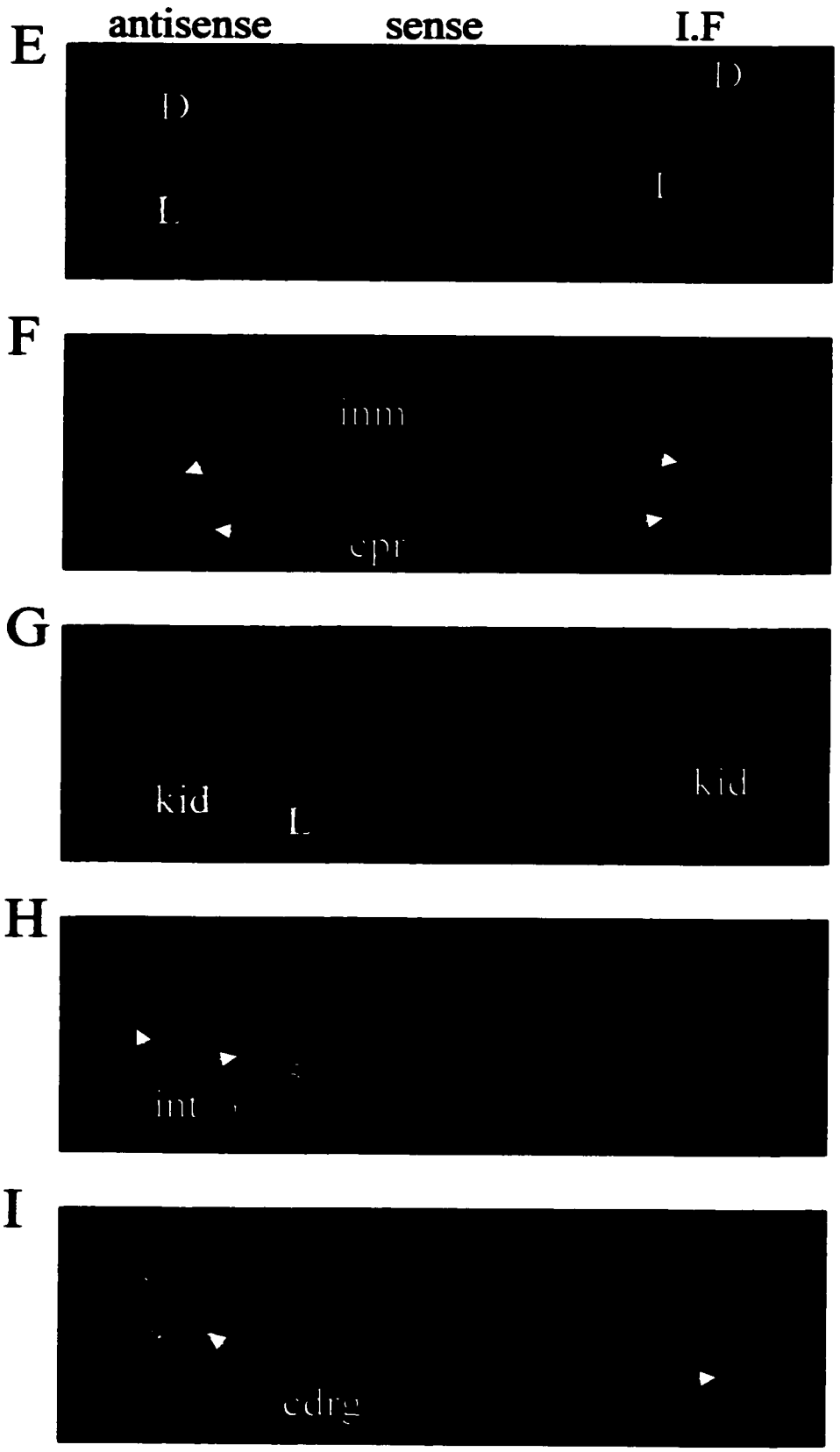
E
antisense
sense
I.F
D
D
I
L
F
imm
epr
G
kid
kid
L
H
int
I
cdrg

and maxillary components showed less expression (Figure 13A and B). Other tissues included, the liver (L), diaphragm (d), intercostal muscles (inm) and cartilage primordium of the ribs (cpr), and kidney (kid) (Figure 13E to G). In contrast, certain E16.5 tissues had displayed a similar level of expression observed at E13.5, for example, the lung (lu), thymus (thy), epithelial cells of the intestinal villi (int), and cervical dorsal root ganglia (cdrg) were amongst those tissues (Figure 13C, D, H, and I).

## 4. Discussion

*Miap3* is expressed during early murine development

The appearance of *miap3* RNA during early murine embryogenesis was validated by RT-PCR, using primers that encompassed a portion of *miap3*. The *miap3* message was first detected at embryonic day 7 (E7) and also later at E11. Since expression was identified relatively early during development, the possibility exists that *miap3* exerts an anti-apoptotic effect early on. Specific localization studies were then done to determine which murine tissues expressed MIAP3.

Identification of *miap3* transcripts with whole-mount *in situ* hybridization (WMISH)

WMISH studies demonstrated that the *miap3* gene exhibits notable patterns of developmental stage-specific expression in a variety of embryonic mouse tissues. Using a DIG-labeled *miap3*-specific probe on mouse embryos from E9.5 to E12, *miap3* transcript was widely distributed in the developing central nervous system (CNS) and to varying degrees in the peripheral nervous system (PNS) (Figure 5-6A and B), suggesting a role for *miap3* in neuronal development. Other developing organs expressing *miap3* transcript included the wall of the heart, developing mandible, liver primordium, developing intestines, neuroepithelium of the neural tube, forelimb and hindlimb buds. However, the exact cellular location of *miap3* expression was not immediately evident. Therefore, whole-mount *miap3* labeled embryos were sectioned. However, the *miap3* signal appeared extremely faint using DIG labelling. Also, following sectioning, the positive control probe, *myogenin*, which gave a strong signal following whole-mount, was barely visible. Increasing colour substrates (BCIP/NBT) only added more background to the embryos, and was therefore reduced to a level that was optimal for whole-mount use. In

light of these problems, *in situ* hybridization with $^{33}P$ labeled riboprobes was used instead.

*Miap3* expression in the developing CNS and PNS

RNA probes radiolabeled with $^{33}P$ were used to identify structures or tissues of the developing mouse embryo that bear *miap3* transcript. Various sections from mouse embryos of E9.5 to E16.5 were analyzed for the temporal and spatial expression patterns of *miap3*.

At all the embryonic stages examined, *miap3* was widely distributed in the developing CNS, although at slightly lower levels during later stages (E16.5). These results suggest a potential role for *miap3* in brain development. *Miap3* transcript, as well as protein, was observed in the neuroepithelium of the telencephalon, mesencephalon and fourth ventricle of embryos from E9.5 to E13.5 (Figures 7A-C). During E16.5 the expression had diminished to a varying degree in the CNS, however it had remained in the same regions observed at earlier times. However, areas staining for *miap3* transcript and protein early on (specifically, the neuroepithelium of telencephalon, mesencephalon, and $4^{th}$ ventricle) had subsequently differentiated into distinct regions of the brain by later time points (Figure 7D). Interestingly, *miap3* was prominently located throughout the developing cortex beginning at E13.5, that is, in the ventricular zone, intermediate zone, and cortical plate. The former is a layer that plays a positive role in the establishment of the definitive cortex and is comprised of postmitotic neurons (Naruse and Keino, 1995). In addition, the intermediate zone is composed of a transitory neuronal layer that is gradually quelled by apoptosis near the time of birth, suggesting a role for *xiap* in its maintenance until parturition (Naruse and Keino, 1995). The number of dead cells at

E10.5 is quite low in the developing cortex of the mouse, however the number increases to seventy percent by mid gestation. Nevertheless, the amount is reduced to half by the end stages of embryogenesis (Blaschke et al., 1996). Furthermore, the expiring cells are most notably observed in the proliferative zones rather than the postmitotic regions.

The distribution of anti-apoptotic proteins BCL-2 and A1 has been observed in multiple tissues during murine embryonic development. For example, in the developing cortical plate BCL-2 and A1 expression appears to be highest at E14.5 (Novack and Korsmeyer, 1994; Carrio et al., 1996). However, their expression was found to be absent from the site associated with extensive cell death, the intermediate zone, and was retained in the proliferating areas of the developing cortex. Therefore, it is reasonable to assume that *bcl-2* and *A1* are involved in brain development (Carrio et al., 1996). Interestingly, MIAP3 was observed at the same time points (E13.5 to E14.5) in similar regions of the brain as BCL-2 and A1. However, MIAP3 expression at E14.5 was more uniformly distributed among the three areas, with overall expression diminishing by E16.5. Therefore, it is possible that MIAP3 is preventing cell death in the regions of the developing cortex, also known to express BCL-2 and A1. In addition, MIAP3 expression was also evident in the intermediate zone, initially at higher levels (E11) (Figure 10A), but reduced by E14 (Figure 7D). This waning of MIAP3 expression in the intermediate zone throughout brain development suggests that loss of expression of this anti-apoptotic protein may contribute to the death of this layer late in development.

Caspase-3 has also been found to be localized in the developing cerebral cortex. More specifically, caspase-3 mRNA was strongly expressed in postmitotic neurons of the cortical plate at E18.5. However, there was no appearance of activated caspase-3 protein

in the cortical plate and thus no apoptotic cells. (Urase et al., 1998). Significantly, activation of caspase-3 protein appears to be implicated in the apoptosis of neuroepithelial cells at E10.5-11.5 and in undifferentiated proliferating neurons of mice at E18.5 (Urase et al., 1998). Caspase-3 null mice exhibit an abundance of cells in their CNS from E12 to E14, evidently due to the reduction in apoptosis of neuroepithelial cells (Kuida et al., 1996). This would imply that caspase-3 is significantly involved with morphogenesis of the CNS in association with apoptosis. With respect to the lack of activated caspase-3 in the cortical plate of E18.5 mice, it is conceivable that the presence of XIAP in the cortical plate is capable of preventing the activation of caspase-3 by protecting the cleavage site of this protease (Nicholson et al., 1995). Furthermore, a threshold level for XIAP may be required to prevent caspase-3 activation (Deveraux and Reed, 1999). When XIAP levels fall below this threshold, caspase-3 becomes vulnerable to cleavage and activation, which can then lead to XIAP cleavage by caspase-3 (Deveraux et al, 1999) ultimately resulting in complete caspase-3 activation and cell death.

Localization of *miap3* in the developing spine

A notable amount of cell death occurs between E13 to E18 in the spinal neurons of the mouse (Lance-Jones, 1982). Interestingly, *miap3* transcript and protein were detected from E9.5 to E13.5 in the neuroepithelium of the spinal cord and neural tube. The expression was also apparent in the mantle layer of the spinal cord in hemi-sectioned mouse embryos of E11.5-12 by WMISH. The expression of *miap3* in the developing spine decreases at around E16.5 (Figure 7D), however, other anti-apoptotic proteins such as BCL-2, are heterogeneously expressed in many cells throughout the mantle layer of

the spinal chord at this stage (Merry et al, 1994). For example, BCL-2 expression is relatively high in alpha motor neurons in comparison to other spinal neurons around E13.5-18.5. In addition, BCL-2 expression in these neurons at E18.5 is essentially the same as that seen at E16.5. The exact neuronal cells expressing MIAP3 were not identified, but it is possible that BCL-2 expression marks specific spinal neurons for survival while diminishing XIAP expression from E13.5 onwards leaves the remaining cells vulnerable to culling by apoptosis. Careful study of *miap3* deficient mice will aid in establishing a role for this protein in brain development.

*Miap3* is expressed in the developing dorsal root ganglion

*Survivin* and Bcl-2 transcript and protein expression is prominent in the neural crest derived cells of the murine dorsal root ganglion (LeBrun et al., 1993; Novack and Korsmeyer, 1994; Adida et al., 1998). More specifically, BCL-2 was detected from E12.5 to E18.5, a period of active cell death (Jacobson, 1991), as well as postnatally, whereas, *survivin* appeared at E15 to E21. *Miap3* was present in the dorsal root ganglion during E11 to E16.5 (Figure's 7D, 8E, 9E, 10H, and 11I) however, the intensity of *miap3* transcript and protein had decreased at E16.5. Interestingly, the caspase-3 transcript was detected in a consistent and intense manner in the mouse dorsal root ganglia at E10.5 but preceded (before E11.5) the appearance of activated caspase-3 and apoptotic cells. In addition, the temporal appearance of the activated caspase-3 in cells of the dorsal root ganglia was consistent with the appearance of apoptotic cells (Urase et al., 1998). Again, loss of MIAP3 expression in a neuronal structure correlates with activation of caspase-3 and induction of cell death, suggesting that MIAP3 is crucial in promoting survival of neurons in earlier developmental stages. Interestingly, the overexpression of XIAP can

inhibit neuronal cell death following ischaemic insult to rat brains, demonstrating the cytoprotective functionality of XIAP in the neuronal context *in vivo* (Xu et al 1997).

*Miap3* in other tissues of the developing mouse embryo

*Miap3* expression was also observed in the developing neurosensory epithelia of the nose and eye. At E13.5, *miap3* transcript and protein localized to the olfactory epithelium (Figure 12C). During early mouse development, the nasal process had almost invariably showed scattered expression of *miap3*, while at E16.5, *miap3* was expressed in the follicles of vibrissae associated with the upper lip. However, expression was less intense than that observed at earlier stages. Interestingly, apoptosis has been well documented in the nasal epithelium as recent as E10.5 (Grindley et al., 1995), when *miap3* is relatively abundant. However, the exact location and role of *miap3* in this organ has not yet been elucidated. *Miap3* transcript and protein were also observed in the developing mouse eye at E13.5. More specifically, expression was scattered throughout the neural and pigmented layer of the retina, as well as in the lens. In addition, particularly high levels of MIAP3 protein versus transcript were apparent in the lens (Figure 12D), suggesting increased translation of MIAP3 or extraordinary stability of MIAP3 protein in this tissue. It is well established that cell death in the mouse retina occurs during normal development as well as in the first two weeks after birth (Young et al., 1984). Therefore, examining the expression of *miap3* in detail in the postnatal retina might prove to be fascinating. Also, caspase-3 is required for normal eye development, as nullizygous mice develop protrusions of the neuroepithelium in the retina due to reduced cell death in this tissue (Kuida et al., 1996). Thus, a balance of caspase-3 and *xiap* in cells of the retina may be critical to the proper development of this tissue.

*In situ* hybridization and immunofluoresence results at E11 showed identical patterns of MIAP3 localization in the first and second mandibular component of the branchial arch. MIAP3 protein was detected within the cytoplasm, as was the case for all tissues examined (Figure 11M). An epithelial layer initially covers and is thought to play a role in the fusion of the branchial arches, however, this layer is not present in the fusion zone and may be eliminated by apoptosis (Schuler, 1995). Determining in which cell types MIAP3 is expressed may provide insight into its possible role in apoptotic events in the developing branchial arches.

Caspase-8 transcript is extensively expressed from E9.5 to E12.5, with augmented levels observed within the developing heart, limb buds and branchial arches (Varfolomeev et al., 1998). Both *maip3* transcript and protein were observed in these tissues during E9.5 to 12.5 and to a lesser degree at E16.5. In addition, *miap3* protein from adult murine heart appeared lower in comparison to the other tissues examined (Figure 5B). Since caspase-8 deficient mice yielded impaired heart muscle development and eventually the death of mouse embryos by E12.5, determining what role MIAP3 is playing during embryonic heart development may provide some insight into normal cell death in the developing heart.

The pattern of *miap3* expression in the embryonic lung, liver, and kidney was consistent until developmental day 13.5 after which time, transcript and protein levels were considerably lower in intensity (Figure 11C, E, and G). However, the postnatal protein levels from these tissues did not diminish in relation to the other adult mouse tissues examined (Figure 5A). In addition, *survivin* and BCL-2 protein has also been identified in the lung, kidney and liver. BCL-2 was mostly in hematopoietic cells of the

liver with expression ceasing after E12.5, while *survivin* was present in the liver from E15 to E21 (Adida et al., 1998). *Miap3* expression was strong from E10 through E12.5 (Figure 7B and C) but declined by E16. Taken together, this implies an early specialized role for BCL-2 in protecting hematopoietic cells while *miap3* protects early hepatocytes. *Survivin* expression may then play a further protective role after *miap3* levels have declined (Novack and Korsmeyer, 1994; Adida et al., 1998). As observed with MIAP3 expression, BCL-2 levels in the kidney are remarkably reduced at E16.5 compared to E12.5. Interestingly, the loss of *bcl-2* results in renal failure and subsequently death of mice at around two months of age. Obviously there is no redundancy with other anti-apoptotic genes, since renal failure would not result if other genes could rescue *bcl-2* function in the afflicted cells at the appropriate time during development of the kidney.

Another tissue characterized by apoptotic cell death, the thymus, has distinct cortical and medullary regions that contain thymocytes at various stages of maturation (Abbas et al., 1994). Although moderate expression of *miap3* during E14.5 (data not shown) and E16.5 (Figure 13D) was observed in the thymus, the exact cell types expressing *miap3* were not obvious. It is possible *miap3* plays a role similar to *bcl-2* in the negative and positive selection of thymocytes. This has yet to be determined.

A noticeable level of *miap3* expression was detected in the epithelial cells of intestinal villi at E16.5 (Figure 13H), a stage when the intestine is coiled with developing villi. However, Western blot analysis clearly indicates adult intestines lacked MIAP3 expression (Figure 8A). As a result, it is possible that MIAP3 is only required for the development of certain cell types in the intestine. The fact that it is expressed embryonically and not in the adult may indicate a general reqirement for immature cells

to express anti-apoptotic proteins in order to overcome a stage-specific susceptibility to cell death. To ascertain *miap3* function within the intestine, mice deficient for *miap3* may assist in clarifying this issue.

Conclusion

For the most part, *miap3* localization during the development of the mouse embryo is widespread. It is particularly different with respect to the spatial and temporal patterns observed for the anti-apoptotic inhibitors of the BCL-2 family (Novack and Korsmeyer, 1994; Carrio et al., 1996) and IAP member, *survivin* (Adida et al., 1998). In addition to its nearly ubiquitous expression pattern, *miap3* levels are clearly higher at early embryonic stages, suggesting a protective function during the early stages of organogenesis. Although the level of sequence similarity is quite high between *xiap* and the other mammalian IAPs, the fact remains that XIAP is the most potent inhibitor of apoptosis promoting cell survival when overexpressed (LaCasse et al., 1998; Deveraux and Reed, 1999). This suggests that XIAP is unique, since this level of inhibition is not seen with the other IAPs.

To assess the role of *miap3* as a regulator of physiological cell death, our study has demonstrated the spatial and temporal expression pattern of *miap3* in the murine embryo. *Miap3* transcript and protein were located within various developing tissues, parts of which eventually succumb to cell death prior to birth. The near absence of MIAP3 protein in the adult intestines, muscle and the low levels detected in the heart were clearly evident and are contrary to the results observed during murine development. During development, *miap3* was clearly distributed within several tissues and thus would imply its involvement with morphogenesis, in addition to tissue homeostasis. However,

due to the widespread expression of *miap3* in numerous tissues, the function of this gene remains to be interpreted. Interestingly, the developing brain had a somewhat ubiquitous expression during development, with a decrease at E16.5. Nevertheless, the peripheral nervous system continued to express moderate to high levels of *miap3* transcript and protein at this stage and suggests a differential regulation of *miap3* compared with that detected in the neurons of the brain. This suggests the presence of differentially regulated elements involved in *miap3* expression.

The data presented indicates that *miap3* expression is developmentally controlled, however, to elucidate in which developing tissues *miap3* is required during embryogenesis, mice deficient for this gene will have to be studied.

## References


Abbas, K.A., Lichtman, A.H., Jordan, S.P. Cellular and Molecular Immunology(2nd Ed.), Philadelphia, Pennsylvania, (1994) pp. 26-27.

Abrams, J. M., White, K., Fessler, L. I., and Steller, H. (1993). Programmed cell death during Drosophila embryogenesis. Development *117*, 29-43.

Adida, C., Crotty, P. L., McGrath, J., Berrebi, D., Diebold, J., and Altieri, D. C. (1998). Developmentally regulated expression of the novel cancer anti-apoptosis gene survivin in human and mouse differentiation. Am J Pathol *152*, 43-9.

Alnemri, E. S., Livingston, D. J., Nicholson, D. W., Salvesen, G., Thornberry, N. A., Wong, W. W., and Yuan, J. (1996). Human ICE/CED-3 protease nomenclature [letter]. Cell *87*, 171.

Ambrosini, G., Adida, C., and Altieri, D. C. (1997). A novel anti-apoptosis gene, survivin, expressed in cancer and lymphoma. Nat Med *3*, 917-21.

Antonsson, B., and Martinou, J. C. (2000). The Bcl-2 protein family. Exp Cell Res *256*, 50-7.

Bergmann, A., Agapite, J., and Steller, H. (1998). Mechanisms and control of programmed cell death in invertebrates. Oncogene *17*, 3215-23.

Birnbaum, H.C. and Dolly, J. (1979). A rapid alkaline extraction procedure for screening recombinant plasmid DNA. Nucleic Acids Res. *7*, 1513-1523.

Birnbaum, M. J., Clem, R. J., and Miller, L. K. (1994). An apoptosis-inhibiting gene from a nuclear polyhedrosis virus encoding a polypeptide with Cys/His sequence motifs. J Virol *68*, 2521-8.

Blaschke, A. J., Staley, K., and Chun, J. (1996). Widespread programmed cell death in proliferative and postmitotic regions of the fetal cerebral cortex. Development *122*, 1165-74.

Blaschke, A. J., Weiner, J. A., and Chun, J. (1998). Programmed cell death is a universal feature of embryonic and postnatal neuroproliferative regions throughout the central nervous system. J Comp Neurol *396*, 39-50.

Boldin, M. P., Goncharov, T. M., Goltsev, Y. V., and Wallach, D. (1996). Involvement of MACH, a novel MORT1/FADD-interacting protease, in Fas/APO-1- and TNF receptor-induced cell death. Cell *85*, 803-15.

Bump, N. J., Hackett, M., Hugunin, M., Seshagiri, S., Brady, K., Chen, P., Ferenz, C., Franklin, S., Ghayur, T., Li, P., and et al. (1995). Inhibition of ICE family proteases by baculovirus antiapoptotic protein p35. Science *269*, 1885-8.

Carrio, R., Lopez-Hoyos, M., Jimeno, J., Benedict, M. A., Merino, R., Benito, A., Fernandez-Luna, J. L., Nunez, G., Garcia-Porrero, J. A., and Merino, J. (1996). A1 demonstrates restricted tissue distribution during embryonic development and functions to protect against cell death. Am J Pathol *149*, 2133-42.

Cecconi, F., Alvarez-Bolado, G., Meyer, B. I., Roth, K. A., and Gruss, P. (1998). Apaf1 (CED-4 homolog) regulates programmed cell death in mammalian development. Cell *94*, 727-37.

Chen, P., Nordstrom, W., Gish, B., and Abrams, J. M. (1996). grim, a novel cell death gene in Drosophila. Genes Dev *10*, 1773-82.

Chen, P., Rodriguez, A., Erskine, R., Thach, T., and Abrams, J. M. (1998). Dredd, a novel effector of the apoptosis activators reaper, grim, and hid in Drosophila. Dev Biol *201*, 202-16.

Chu, Z. L., McKinsey, T. A., Liu, L., Gentry, J. J., Malim, M. H., and Ballard, D. W. (1997). Suppression of tumor necrosis factor-induced cell death by inhibitor of apoptosis c-IAP2 is under NF-kappaB control. Proc Natl Acad Sci U S A *94*, 10057-62.

Clem, R. J., and Miller, L. K. (1994). Control of programmed cell death by the baculovirus genes p35 and iap. Mol Cell Biol *14*, 5212-22.

Conradt, B., and Horvitz, H. R. (1998). The C. elegans protein EGL-1 is required for programmed cell death and interacts with the Bcl-2-like protein CED-9. Cell *93*, 519-29.

Coucouvanis, E., and Martin, G. R. (1995). Signals for death and survival: a two-step mechanism for cavitation in the vertebrate embryo. Cell *83*, 279-87.

Crook, N. E., Clem, R. J., and Miller, L. K. (1993). An apoptosis-inhibiting baculovirus gene with a zinc finger-like motif. J Virol *67*, 2168-74.

Deveraux, Q. L., Leo, E., Stennicke, H. R., Welsh, K., Salvesen, G. S., and Reed, J. C. (1999). Cleavage of human inhibitor of apoptosis protein XIAP results in fragments with distinct specificities for caspases. Embo J *18*, 5242-51.

Deveraux, Q. L., and Reed, J. C. (1999). IAP family proteins--suppressors of apoptosis. Genes Dev *13*, 239-52.

Deveraux, Q. L., Roy, N., Stennicke, H. R., Van Arsdale, T., Zhou, Q., Srinivasula, S. M., Alnemri, E. S., Salvesen, G. S., and Reed, J. C. (1998). IAPs block apoptotic events

induced by caspase-8 and cytochrome c by direct inhibition of distinct caspases. Embo J *17*, 2215-23.

Deveraux, Q. L., Takahashi, R., Salvesen, G. S., and Reed, J. C. (1997). X-linked IAP is a direct inhibitor of cell-death proteases. Nature *388*, 300-4.

Dorstyn, L., Colussi, P. A., Quinn, L. M., Richardson, H., and Kumar, S. (1999). DRONC, an ecdysone-inducible Drosophila caspase. Proc Natl Acad Sci U S A *96*, 4307-12.

Du, C., Fang, M., Li, Y., Li, L., and Wang, X. (2000). Smac, a mitochondrial protein that promotes cytochrome c-dependent caspase activation by eliminating IAP inhibition. Cell *102*, 33-42.

Duckett, C. S., Nava, V. E., Gedrich, R. W., Clem, R. J., Van Dongen, J. L., Gilfillan, M. C., Shiels, H., Hardwick, J. M., and Thompson, C. B. (1996). A conserved family of cellular genes related to the baculovirus iap gene and encoding apoptosis inhibitors. Embo J *15*, 2685-94.

Ellis, H. M., and Horvitz, H. R. (1986). Genetic control of programmed cell death in the nematode C. elegans. Cell *44*, 817-29.

Ellis, R. E., Yuan, J. Y., and Horvitz, H. R. (1991). Mechanisms and functions of cell death. Annu Rev Cell Biol *7*, 663-98.

Farahani, R., Fong, W. G., Korneluk, R. G., and MacKenzie, A. E. (1997). Genomic organization and primary characterization of miap-3: the murine homologue of human X-linked IAP. Genomics *42*, 514-8.

Finucane, D. M., Bossy-Wetzel, E., Waterhouse, N. J., Cotter, T. G., and Green, D. R. (1999). Bax-induced caspase activation and apoptosis via cytochrome c release from mitochondria is inhibitable by Bcl-xL. J Biol Chem *274*, 2225-33.

Fraser, A. G., and Evan, G. I. (1997). Identification of a Drosophila melanogaster ICE/CED-3-related protease, drICE. Embo J *16*, 2805-13.

Freemont, P. S., Hanson, I. M., and Trowsdale, J. (1991). A novel cysteine-rich sequence motif [letter]. Cell *64*, 483-4.

Grether, M. E., Abrams, J. M., Agapite, J., White, K., and Steller, H. (1995). The head involution defective gene of Drosophila melanogaster functions in programmed cell death. Genes Dev *9*, 1694-708.

Grindley, J. C., Davidson, D. R., and Hill, R. E. (1995). The role of Pax-6 in eye and nasal development. Development *121*, 1433-42.

Hakem, R., Hakem, A., Duncan, G. S., Henderson, J. T., Woo, M., Soengas, M. S., Elia, A., de la Pompa, J. L., Kagi, D., Khoo, W., Potter, J., Yoshida, R., Kaufman, S. A., Lowe, S. W., Penninger, J. M., and Mak, T. W. (1998). Differential requirement for caspase 9 in apoptotic pathways in vivo. Cell *94*, 339-52.

Hay, B. A., Wassarman, D. A., and Rubin, G. M. (1995). Drosophila homologs of baculovirus inhibitor of apoptosis proteins function to block cell death. Cell *83*, 1253-62.

Hengartner, M. O., Ellis, R. E., and Horvitz, H. R. (1992). Caenorhabditis elegans gene ced-9 protects cells from programmed cell death. Nature *356*, 494-9.

Hengartner, M. O., and Horvitz, H. R. (1994). C. elegans cell survival gene ced-9 encodes a functional homolog of the mammalian proto-oncogene bcl-2. Cell *76*, 665-76.

Hockenbery, D. M., Zutter, M., Hickey, W., Nahm, M., and Korsmeyer, S. J. (1991). BCL2 protein is topographically restricted in tissues characterized by apoptotic cell death. Proc Natl Acad Sci U S A *88*, 6961-5.

Hofmann, K., Bucher, P., and Tschopp, J. (1997). The CARD domain: a new apoptotic signalling motif. Trends Biochem Sci *22*, 155-6.

Holcik, M., Lefebvre, C., Yeh, C., Chow, T., and Korneluk, R. G. (1999). A new internal-ribosome-entry-site motif potentiates XIAP-mediated cytoprotection. Nat Cell Biol *1*, 190-2.

Horvitz, H. R., Chalfie, M., Trent, C., Sulston, J. E., and Evans, P. D. (1982). Serotonin and octopamine in the nematode Caenorhabditis elegans. Science *216*, 1012-4.

Hsu, Y. T., Wolter, K. G., and Youle, R. J. (1997). Cytosol-to-membrane redistribution of Bax and Bcl-X(L) during apoptosis. Proc Natl Acad Sci U S A *94*, 3668-72.

Inohara, N., Koseki, T., Hu, Y., Chen, S., and Nunez, G. (1997). CLARP, a death effector domain-containing protein interacts with caspase-8 and regulates apoptosis. Proc Natl Acad Sci U S A *94*, 10717-22.

Jacobson, M. (1991). Developmental Neurobiology. New York: Plenum Press. pp 451-475.

Jacobson, M. D., Weil, M., and Raff, M. C. (1997). Programmed cell death in animal development. Cell *88*, 347-54.

Kerr, J. F., Wyllie, A. H., and Currie, A. R. (1972). Apoptosis: a basic biological phenomenon with wide-ranging implications in tissue kinetics. Br J Cancer *26*, 239-57.

Kluck, R. M., Bossy-Wetzel, E., Green, D. R., and Newmeyer, D. D. (1997). The release of cytochrome c from mitochondria: a primary site for Bcl-2 regulation of apoptosis [see comments]. Science *275*, 1132-6.

Knudson, C. M., Tung, K. S., Tourtellotte, W. G., Brown, G. A., and Korsmeyer, S. J. (1995). Bax-deficient mice with lymphoid hyperplasia and male germ cell death. Science *270*, 96-9.

Korsmeyer, S. J. (1995). Regulators of cell death. Trends Genet *11*, 101-5.

Krajewski, S., Tanaka, S., Takayama, S., Schibler, M. J., Fenton, W., and Reed, J. C. (1993). Investigation of the subcellular distribution of the bcl-2 oncoprotein: residence in the nuclear envelope, endoplasmic reticulum, and outer mitochondrial membranes. Cancer Res *53*, 4701-14.

Kuida, K., Haydar, T. F., Kuan, C. Y., Gu, Y., Taya, C., Karasuyama, H., Su, M. S., Rakic, P., and Flavell, R. A. (1998). Reduced apoptosis and cytochrome c-mediated caspase activation in mice lacking caspase 9. Cell *94*, 325-37.

Kuida, K., Zheng, T. S., Na, S., Kuan, C., Yang, D., Karasuyama, H., Rakic, P., and Flavell, R. A. (1996). Decreased apoptosis in the brain and premature lethality in CPP32-deficient mice. Nature *384*, 368-72.

Kumar, S. (1999). Mechanisms mediating caspase activation in cell death. Cell Death Differ *6*, 1060-6.

Kumar, S., and Colussi, P. A. (1999). Prodomains--adaptors--oligomerization: the pursuit of caspase activation in apoptosis. Trends Biochem Sci *24*, 1-4.

LaCasse, E. C., Baird, S., Korneluk, R. G., and MacKenzie, A. E. (1998). The inhibitors of apoptosis (IAPs) and their emerging role in cancer. Oncogene *17*, 3247-59.

Lance-Jones, C. (1982). Motoneuron cell death in the developing lumbar spinal cord of the mouse. Brain Res *256*, 473-9.

LeBrun, D. P., Warnke, R. A., and Cleary, M. L. (1993). Expression of bcl-2 in fetal tissues suggests a role in morphogenesis. Am J Pathol *142*, 743-53.

Li, J., Kim, J. M., Liston, P., Li, M., Miyazaki, T., Mackenzie, A. E., Korneluk, R. G., and Tsang, B. K. (1998). Expression of inhibitor of apoptosis proteins (IAPs) in rat granulosa cells during ovarian follicular development and atresia. Endocrinology *139*, 1321-8.

Li, P., Nijhawan, D., Budihardjo, I., Srinivasula, S. M., Ahmad, M., Alnemri, E. S., and Wang, X. (1997). Cytochrome c and dATP-dependent formation of Apaf-1/caspase-9 complex initiates an apoptotic protease cascade. Cell *91*, 479-89.

Liston, P., Roy, N., Tamai, K., Lefebvre, C., Baird, S., Cherton-Horvat, G., Farahani, R., McLean, M., Ikeda, J. E., MacKenzie, A., and Korneluk, R. G. (1996). Suppression of apoptosis in mammalian cells by NAIP and a related family of IAP genes. Nature *379*, 349-53.

Lockshin, R. A. (1969). Programmed cell death. Activation of lysis by a mechanism involving the synthesis of protein. J Insect Physiol *15*, 1505-16.

McCall, K., and Steller, H. (1998). Requirement for DCP-1 caspase during Drosophila oogenesis. Science *279*, 230-4.

Medema, J. P., Scaffidi, C., Kischkel, F. C., Shevchenko, A., Mann, M., Krammer, P. H., and Peter, M. E. (1997). FLICE is activated by association with the CD95 death-inducing signaling complex (DISC). Embo J *16*, 2794-804.

Meier, P., and Evan, G. (1998). Dying like flies [comment]. Cell *95*, 295-8.

Merry, D. E., Veis, D. J., Hickey, W. F., and Korsmeyer, S. J. (1994). bcl-2 protein expression is widespread in the developing nervous system and retained in the adult PNS. Development *120*, 301-11.

Motoyama, N., Wang, F., Roth, K. A., Sawa, H., Nakayama, K., Negishi, I., Senju, S., Zhang, Q., Fujii, S., and et al. (1995). Massive cell death of immature hematopoietic cells and neurons in Bcl-x-deficient mice. Science *267*, 1506-10.

Mukasa, T., Urase, K., Momoi, M. Y., Kimura, I., and Momoi, T. (1997). Specific expression of CPP32 in sensory neurons of mouse embryos and activation of CPP32 in the apoptosis induced by a withdrawal of NGF. Biochem Biophys Res Commun *231*, 770-4.

Muzio, M., Chinnaiyan, A. M., Kischkel, F. C., O'Rourke, K., Shevchenko, A., Ni, J., Scaffidi, C., Bretz, J. D., Zhang, M., Gentz, R., Mann, M., Krammer, P. H., Peter, M. E., and Dixit, V. M. (1996). FLICE, a novel FADD-homologous ICE/CED-3-like protease, is recruited to the CD95 (Fas/APO-1) death--inducing signaling complex. Cell *85*, 817-27.

Naruse, I., and Keino, H. (1995). Apoptosis in the developing CNS. Prog Neurobiol *47*, 135-55.

Nicholson, D. W., Ali, A., Thornberry, N. A., Vaillancourt, J. P., Ding, C. K., Gallant, M., Gareau, Y., Griffin, P. R., Labelle, M., Lazebnik, Y. A., and et al. (1995). Identification and inhibition of the ICE/CED-3 protease necessary for mammalian apoptosis [see comments]. Nature *376*, 37-43.

Nicholson, D. W., and Thornberry, N. A. (1997). Caspases: killer proteases. Trends Biochem Sci *22*, 299-306.

Novack, D. V., and Korsmeyer, S. J. (1994). Bcl-2 protein expression during murine development [see comments]. Am J Pathol *145*, 61-73.

Oeda, E., Oka, Y., Miyazono, K., and Kawabata, M. (1998). Interaction of Drosophila inhibitors of apoptosis with thick veins, a type I serine/threonine kinase receptor for decapentaplegic. J Biol Chem *273*, 9353-6.

Oltvai, Z. N., and Korsmeyer, S. J. (1994). Checkpoints of dueling dimers foil death wishes [comment]. Cell *79*, 189-92.

Oppenheim, R. W. (1991). Cell death during development of the nervous system. Annu Rev Neurosci *14*, 453-501.

Oppenheim, R. W., Prevette, D., Tytell, M., and Homma, S. (1990). Naturally occurring and induced neuronal death in the chick embryo in vivo requires protein and RNA synthesis: evidence for the role of cell death genes. Dev Biol *138*, 104-13.

Perez, G. I., Knudson, C. M., Leykin, L., Korsmeyer, S. J., and Tilly, J. L. (1997). Apoptosis-associated signaling pathways are required for chemotherapy-mediated female germ cell destruction [see comments]. Nat Med *3*, 1228-32.

Rajcan-Separovic, E., Liston, P., Lefebvre, C., and Korneluk, R. G. (1996). Assignment of human inhibitor of apoptosis protein (IAP) genes xiap, hiap-1, and hiap-2 to chromosomes Xq25 and 11q22-q23 by fluorescence in situ hybridization. Genomics *37*, 404-6.

Rathmell, J. C., and Thompson, C. B. (1999). The central effectors of cell death in the immune system. Annu Rev Immunol *17*, 781-828.

Rothe, M., Pan, M. G., Henzel, W. J., Ayres, T. M., and Goeddel, D. V. (1995). The TNFR2-TRAF signaling complex contains two novel proteins related to baculoviral inhibitor of apoptosis proteins. Cell *83*, 1243-52.

Roy, N., Deveraux, Q. L., Takahashi, R., Salvesen, G. S., and Reed, J. C. (1997). The c-IAP-1 and c-IAP-2 proteins are direct inhibitors of specific caspases. Embo J *16*, 6914-25.

Roy, N., McLean, M. D., Besner-Johnston, A., Lefebvre, C., Salih, M., Carpten, J. D., Burghes, A. H., Yaraghi, Z., Ikeda, J. E., Korneluk, R. G., and et al. (1995). Refined physical map of the spinal muscular atrophy gene (SMA) region at 5q13 based on YAC and cosmid contiguous arrays. Genomics *26*, 451-60.

Sambrook, J., Fritsch, E.F. & Maniatis, T. Molecular Cloning: A Laboratory Manual (2nd Ed.), Cold Spring Harbor, NY, (1989).

Sassoon, D., Lyons, G., Wright, W. E., Lin, V., Lassar, A., Weintraub, H., and Buckingham, M. (1989). Expression of two myogenic regulatory factors myogenin and MyoD1 during mouse embryogenesis. Nature *341*, 303-7.

Shuler, C. F. (1995). Programmed cell death and cell transformation in craniofacial development. Crit Rev Oral Biol Med *6*, 202-17.

Song, Z., McCall, K., and Steller, H. (1997). DCP-1, a Drosophila cell death protease essential for development [published erratum appears in Science 1997 Jul 11;277(5323):167]. Science *275*, 536-40.

Srinivasula, S. M., Ahmad, M., Fernandes-Alnemri, T., and Alnemri, E. S. (1998). Autoactivation of procaspase-9 by Apaf-1-mediated oligomerization. Mol Cell *1*, 949-57.

Stehlik, C., de Martin, R., Kumabashiri, I., Schmid, J. A., Binder, B. R., and Lipp, J. (1998). Nuclear factor (NF)-kappaB-regulated X-chromosome-linked iap gene expression protects endothelial cells from tumor necrosis factor alpha-induced apoptosis. J Exp Med *188*, 211-6.

Stennicke, H. R., Jurgensmeier, J. M., Shin, H., Deveraux, Q., Wolf, B. B., Yang, X., Zhou, Q., Ellerby, H. M., Ellerby, L. M., Bredesen, D., Green, D. R., Reed, J. C., Froelich, C. J., and Salvesen, G. S. (1998). Pro-caspase-3 is a major physiologic target of caspase-8. J Biol Chem *273*, 27084-90.

Takahashi, A., Alnemri, E. S., Lazebnik, Y. A., Fernandes-Alnemri, T., Litwack, G., Moir, R. D., Goldman, R. D., Poirier, G. G., Kaufmann, S. H., and Earnshaw, W. C. (1996). Cleavage of lamin A by Mch2 alpha but not CPP32: multiple interleukin 1 beta-converting enzyme-related proteases with distinct substrate recognition properties are active in apoptosis. Proc Natl Acad Sci U S A *93*, 8395-400.

Takahashi, R., Deveraux, Q., Tamm, I., Welsh, K., Assa-Munt, N., Salvesen, G. S., and Reed, J. C. (1998). A single BIR domain of XIAP sufficient for inhibiting caspases. J Biol Chem *273*, 7787-90.

Tamm, I., Wang, Y., Sausville, E., Scudiero, D. A., Vigna, N., Oltersdorf, T., and Reed, J. C. (1998). IAP-family protein survivin inhibits caspase activity and apoptosis induced by Fas (CD95), Bax, caspases, and anticancer drugs. Cancer Res *58*, 5315-20.

Tata, J. R. (1966). Requirement for RNA and protein synthesis for induced regression of the tadpole tail in organ culture. Dev Biol *13*, 77-94.

Thompson, C. B. (1995). Apoptosis in the pathogenesis and treatment of disease. Science *267*, 1456-62.

Tsujimoto, Y., Gorham, J., Cossman, J., Jaffe, E., and Croce, C. M. (1985). The t(14;18) chromosome translocations involved in B-cell neoplasms result from mistakes in VDJ joining. Science *229*, 1390-3.

Urase, K., Fujita, E., Miho, Y., Kouroku, Y., Mukasa, T., Yagi, Y., Momoi, M. Y., and Momoi, T. (1998). Detection of activated caspase-3 (CPP32) in the vertebrate nervous system during development by a cleavage site-directed antiserum. Brain Res Dev Brain Res *111*, 77-87.

Uren, A. G., Pakusch, M., Hawkins, C. J., Puls, K. L., and Vaux, D. L. (1996). Cloning and expression of apoptosis inhibitory protein homologs that function to inhibit apoptosis and/or bind tumor necrosis factor receptor-associated factors. Proc Natl Acad Sci U S A *93*, 4974-8.

Varfolomeev, E. E., Schuchmann, M., Luria, V., Chiannilkulchai, N., Beckmann, J. S., Mett, I. L., Rebrikov, D., Brodianski, V. M., Kemper, O. C., Kollet, O., Lapidot, T., Soffer, D., Sobe, T., Avraham, K. B., Goncharov, T., Holtmann, H., Lonai, P., and Wallach, D. (1998). Targeted disruption of the mouse Caspase 8 gene ablates cell death induction by the TNF receptors, Fas/Apo1, and DR3 and is lethal prenatally. Immunity *9*, 267-76.

Vaux, D. L., Cory, S., and Adams, J. M. (1988). Bcl-2 gene promotes haemopoietic cell survival and cooperates with c-myc to immortalize pre-B cells. Nature *335*, 440-2.

Vaux, D. L., and Korsmeyer, S. J. (1999). Cell death in development. Cell *96*, 245-54.

Vaux, D. L., Weissman, I. L., and Kim, S. K. (1992). Prevention of programmed cell death in Caenorhabditis elegans by human bcl-2. Science *258*, 1955-7.

Veis, D. J., Sorenson, C. M., Shutter, J. R., and Korsmeyer, S. J. (1993). Bcl-2-deficient mice demonstrate fulminant lymphoid apoptosis, polycystic kidneys, and hypopigmented hair. Cell *75*, 229-40.

Vucic, D., Kaiser, W. J., Harvey, A. J., and Miller, L. K. (1997). Inhibition of reaper-induced apoptosis by interaction with inhibitor of apoptosis proteins (IAPs). Proc Natl Acad Sci U S A *94*, 10183-8.

Vucic, D., Kaiser, W. J., and Miller, L. K. (1998). Inhibitor of apoptosis proteins physically interact with and block apoptosis induced by Drosophila proteins HID and GRIM. Mol Cell Biol *18*, 3300-9.

White, K., Grether, M. E., Abrams, J. M., Young, L., Farrell, K., and Steller, H. (1994). Genetic control of programmed cell death in Drosophila [see comments]. Science *264*, 677-83.

White, K., Tahaoglu, E., and Steller, H. (1996). Cell killing by the Drosophila gene reaper. Science *271*, 805-7.

Woo, M., Hakem, R., Soengas, M. S., Duncan, G. S., Shahinian, A., Kagi, D., Hakem, A., McCurrach, M., Khoo, W., Kaufman, S. A., Senaldi, G., Howard, T., Lowe, S. W., and Mak, T. W. (1998). Essential contribution of caspase 3/CPP32 to apoptosis and its associated nuclear changes. Genes Dev *12*, 806-19.

Wyllie, A. H., Kerr, J. F., and Currie, A. R. (1980). Cell death: the significance of apoptosis. Int Rev Cytol *68*, 251-306.

Xu, D., Bureau, Y., McIntyre, D. C., Nicholson, D. W., Liston, P., Zhu, Y., Fong, W. G., Crocker, S. J., Korneluk, R. G., and Robertson, G. S. (1999). Attenuation of ischemia-induced cellular and behavioral deficits by X chromosome-linked inhibitor of apoptosis protein overexpression in the rat hippocampus. J Neurosci *19*, 5026-33.

Xu, D. G., Crocker, S. J., Doucet, J. P., St-Jean, M., Tamai, K., Hakim, A. M., Ikeda, J. E., Liston, P., Thompson, C. S., Korneluk, R. G., MacKenzie, A., and Robertson, G. S. (1997). Elevation of neuronal expression of NAIP reduces ischemic damage in the rat hippocampus. Nat Med *3*, 997-1004.

Xue, D., and Horvitz, H. R. (1995). Inhibition of the Caenorhabditis elegans cell-death protease CED-3 by a CED-3 cleavage site in baculovirus p35 protein. Nature *377*, 248-51.

Yamaguchi, K., Nagai, S., Ninomiya-Tsuji, J., Nishita, M., Tamai, K., Irie, K., Ueno, N., Nishida, E., Shibuya, H., and Matsumoto, K. (1999). XIAP, a cellular member of the inhibitor of apoptosis protein family, links the receptors to TAB1-TAK1 in the BMP signaling pathway. Embo J *18*, 179-87.

Yang, E., and Korsmeyer, S. J. (1996). Molecular thanatopsis: a discourse on the BCL2 family and cell death. Blood *88*, 386-401.

Yeh, W. C., Pompa, J. L., McCurrach, M. E., Shu, H. B., Elia, A. J., Shahinian, A., Ng, M., Wakeham, A., Khoo, W., Mitchell, K., El-Deiry, W. S., Lowe, S. W., Goeddel, D. V., and Mak, T. W. (1998). FADD: essential for embryo development and signaling from some, but not all, inducers of apoptosis. Science *279*, 1954-8.

Yoshida, H., Kong, Y. Y., Yoshida, R., Elia, A. J., Hakem, A., Hakem, R., Penninger, J. M., and Mak, T. W. (1998). Apaf1 is required for mitochondrial pathways of apoptosis and brain development. Cell *94*, 739-50.

Young, R. W. (1984). Cell death during differentiation of the retina in the mouse. J Comp Neurol *229*, 362-73.

Yuan, J., and Horvitz, H. R. (1992). The Caenorhabditis elegans cell death gene ced-4 encodes a novel protein and is expressed during the period of extensive programmed cell death. Development *116*, 309-20.

Yuan, J., Shaham, S., Ledoux, S., Ellis, H. M., and Horvitz, H. R. (1993). The C. elegans cell death gene ced-3 encodes a protein similar to mammalian interleukin-1 beta-converting enzyme. Cell *75*, 641-52.

Zakeri, Z. F., and Ahuja, H. S. (1994). Apoptotic cell death in the limb and its relationship to pattern formation. Biochem Cell Biol *72*, 603-13.